Structures 70 (2024) 107898

Contents lists available at ScienceDirect

Structures

journal homepage: www.elsevier.com/locate/structures

Practical methodology for quantifying the structural robustness of RC building structures

Andri Setiawan *, Diego Cetina, Nirvan Makoond, Manuel Buitrago, Jose M. Adam

ICITECH, Universitat Politècnica de València, Camino de Vera s/n, Valencia 46022, Spain

ARTICLE INFO

Keywords:
Building structures
Progressive collapse
Structural robustness
Computational modelling
Robustness index

ABSTRACT

Several structural robustness requirements have been included in building codes over the past two decades. These mainly include measures to prevent collapse after an initial component failure by ensuring a minimum level of continuity within the structural system so that loads supported by the failed component can be redistributed to the rest of the structural system. However, there is still a general lack of consensus on how to evaluate the effectiveness of these measures. The present study proposes a practical methodology to evaluate the structural robustness of RC building structures by combining an efficient modelling strategy and suitable robustness indexes. The proposed computational modelling strategy for RC buildings accounts for relevant dynamic and nonlinear phenomena, including compressive arching, catenary action, and membrane effects. This strategy can be implemented at a reasonable computational expense in widely used commercial structural analysis software and has been validated by comparisons to selected experimental tests from the literature. The modelling strategy is then employed to compute four different robustness indexes proposed in the literature for three hypothetical building designs, allowing the indexes to be systematically compared. It was found that evaluating a system using multiple robustness indexes can provide a more holistic view of system performance compared to relying solely on a single index. Ultimately, the potential usefulness of the proposed methodology is demonstrated through two practical applications involving the estimation of component damage levels and the evaluation of different design and retrofitting solutions. Such a methodology can be useful for practising engineers to optimise the design of new buildings or to support decisions on the assessment and retrofitting of existing ones.

1. Introduction

The need to design robust buildings that are insensitive to initial local failures is now widely recognised as a key aspect of societal resilience [1]. Indeed, there has been a significant research effort over the past five decades to better understand progressive collapse and how to prevent it [2,3]. This has led to the inclusion in building codes of several prescriptive and pragmatic approaches to improve structural robustness [4–7]. Most of these approaches rely on ensuring that alternative load paths (ALPs) are available after the loss of load-bearing elements so that the load supported by these elements can be redistributed to other parts of the structure. Although this strategy has proven to work effectively in several situations [8], there is still a general lack of consensus on how to evaluate the effectiveness of applying these measures in buildings with different characteristics [3,9,10]. Evaluating the effectiveness of designs with respect to structural robustness requires overcoming two principal challenges: (i) developing a practical and cost-effective computational modelling strategy that is sufficiently accurate for simulating extreme scenarios and (ii) verifying the expressiveness and applicability of quantitative robustness indexes proposed in the literature for different design situations.

The response of building structures after the loss of load-bearing elements involves dynamic effects and nonlinear material behaviour that sometimes lead to large displacements, making it difficult to ensure the reliability of simulations at a reasonable computational cost. Nevertheless, different modelling strategies (Fig. 1) have been proposed for simulating the behaviour of reinforced concrete (RC) framed buildings after the loss of columns [11]. It is crucial to consider nonlinear material responses to avoid inefficient design solutions that are based on inaccurate representations of stress redistribution. Such considerations can be implemented in line elements either using lumped-hinge models (Fig. 1a) or models with distributed fibre sections (Fig. 1b) [11]. Several studies [12–17] employ such approaches, often relying only on bare-frame models that completely neglect the contribution of slabs.

* Corresponding author.
E-mail address: asetiaw1@upvnet.upv.es (A. Setiawan).

https://doi.org/10.1016/j.istruc.2024.107898
Received 27 June 2024; Received in revised form 19 November 2024; Accepted 21 November 2024

While meaningful conclusions can still be drawn using such models, it is now well-recognised that membrane actions in slabs contribute significantly to progressive collapse resistance [3,11,18] and that they should, therefore, be considered to produce accurate simulations. To address this issue, some researchers have improved bare-frame models using grillage representations of the floor system [14] or multilayered shells (Fig. 1c) [17]. Finally, highly accurate simulations can be performed using solid elements [11,17,19], but these are typically too computationally expensive to be used for modelling complete building systems in most practical applications (Fig. 1d). It is important to note that the classification shown in Fig. 1 is mostly relevant for strategies based on the finite element method (FEM), which is the most widely used approach for performing simulations in the field of structural engineering. Nevertheless, it should be mentioned that other strategies (employing 3D-solid elements) can be used to simulate progressive collapse, notably the discrete element method (DEM) [20–22] and the applied element method (AEM) [23–27].

In short, a wide variety of modelling approaches have been used successfully to simulate progressive collapse phenomena. Despite this fact, it can still be challenging for practitioners and researchers to build nonlinear models that achieve a suitable balance between accuracy and computational expense.

Even if ALPs after the loss of columns can be accurately simulated, objectively assessing the effectiveness of different design options remains a challenge without a quantitative measure of robustness. Such a measure can take the form of a robustness index and could have several applications beyond serving as a design-aid [9,10,28]. For instance, a suitable index could be used to optimise decisions, as a system partial safety factor, to classify different types of structures, or to specify quantitative robustness requirements in regulations and for project-specific verifications [9]. Several researchers have proposed many different types of robustness indexes [3,9,10,29]. For example, damage-based robustness indexes that involve estimating the extent of collapse are well-suited to evaluate segmentation designs for improving robustness [9,30], while risk-based indexes that allow rigorous consideration of both costs and benefits are well-suited for optimising risk-mitigation decisions. However, both types of indexes can be very challenging to compute: the former due to the difficulty of modelling element separation and impacts, and the latter due to the difficulty of estimating required probabilities. One type of index that is particularly suitable for evaluating the effectiveness of measures (or for comparing design alternatives) that intend to ensure the availability of ALPs are reserve-based indexes, which are based on estimating the remaining load capacity of a structural system after an initial failure [9]. These indexes are not only very practical but are also appropriate for most robustness design methods included in current building codes. Despite this fact, proposed reserve-based robustness indexes have not been subjected to comprehensive scrutiny. In fact, to the best of the authors' knowledge, there are no studies that explicitly compare the application of different reserve-based robustness indexes to different building designs.

The work presented in this article aims to develop a standardised quantitative methodology for assessing the robustness of RC building structures by combining efficient computational modelling strategy and suitable robustness indexes. The first part of the article (Section 2) describes the computationally efficient nonlinear modelling strategy to accurately estimate the behaviour of RC building structures after the loss of load-bearing elements. The modelling strategy is then employed to compute four different reserve-based robustness indexes proposed in literature for three hypothetical building designs (Section 3). First, the consistency between indexes is analysed. The robustness of the three building designs used as case studies is then discussed based on the evaluated indexes, allowing useful conclusions to be drawn on how different building characteristics can influence structural robustness. Finally, two potential applications of the evaluated robustness indexes are explained (Section 4). The demonstrated applications include: (i) estimating the damage state of local structural components involved in the load redistribution process, and (ii) assessing the effectiveness of different design and retrofitting strategies for improving structural robustness.

2. Practical modelling strategy

This section describes the proposed modelling strategy adopted for

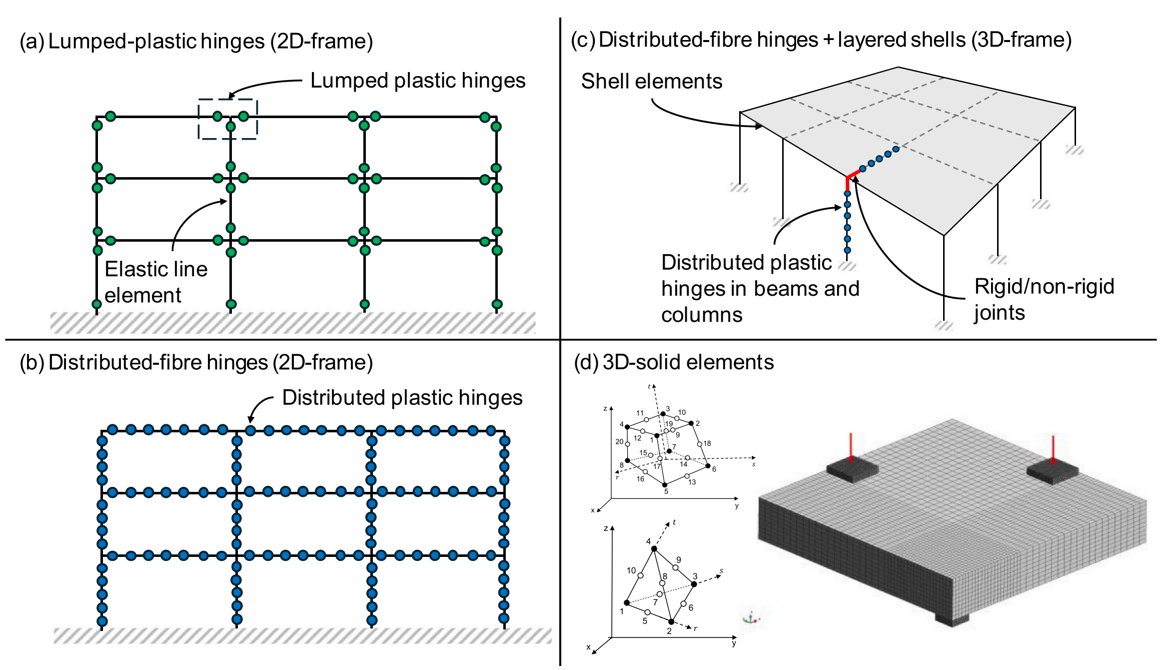

Fig. 1. Different modelling strategies for simulating the progressive collapse of RC structures: (a) 2D-frame with lumped plastic hinges; (b) 2D-frame with distributed plastic hinges; (c) 3D-frame with distributed plastic hinges for the frames and nonlinear layered shells for the slabs (or by using grillage representations); (d) 3D-solid models.

performing the robustness index quantification. To simulate the realistic behaviour of RC structures subjected to progressive collapse, several key aspects are considered: 1) the 3D framing effect; 2) the contribution of floor systems (slab) in providing the alternative load paths; 3) material and geometric nonlinearities accounting for the cracking and crushing of the concrete, yielding, and fracture of the reinforcement bars under large deformations (catenary mechanisms); 4) the dynamic effect that amplifies the forces and deformations experienced by the system when load-bearing elements are removed suddenly. To account for these effects, a practical modelling strategy was proposed based on the following assumptions:

1. Beams and columns are modelled as line elements where nonlinearity due to cracking and reinforcement yielding are represented by the distributed-fibre approach [31]. Such elements consider both material and geometric nonlinearities (large deformations). As will be discussed in Section 2.1, some essential modelling parameters must be properly chosen to ensure reliable results. An alternative approach based on PMM-hinge (lumped), as typically adopted in the earthquake engineering field [32,33], was investigated previously by the authors [34], and it was found to be valid only for small deformations (flexural) but not for larger ones (involving catenary action). Thus, its use is not recommended for simulating column-loss scenarios.
2. Either static or dynamic analysis is used depending on the choice of robustness index or on case-specific needs. When dynamic analysis is performed (as in Sections 2.2 and 2.3), this study consistently adopts a removal time that is less than one-tenth of the predominant vertical vibration mode of the structural system [6]. A constant viscous (modal) damping of 5 % is adopted for all analyses.
3. To account for the contribution of the floor slabs, two strategies were investigated: a) a simplified grillage (grids of equivalent beams) approach [35] and b) a more refined element formulation based on nonlinear layered shells [36–38]. Section 2.3 discusses this aspect in more detail, and the advantages and disadvantages of each approach are presented.
4. Reinforcement bars are assumed to be perfectly bonded to the concrete (no slip). Shear failure of the beam, splicing or anchorage failure of the rebar, and joint failure are not considered. These can be regarded as a reasonable assumption as the buildings that are investigated in this study are new buildings that are designed with modern codes and comply with a certain level of seismic detailing [39]. Additional analytical checks (through post-processing) can be done to verify the validity of these assumptions, but they are beyond the scope of the present study.

The characteristics of the buildings investigated in the present study focus on a three-dimensional frame system made of cast-in-situ reinforced concrete structures. The systems combine columns, main (primary) beams in both directions and two-way reinforced concrete slabs spanning between primary beams (no secondary beams). Particularly, the focus is on low- to mid-rise type structures where no lateral bracing or wall systems are generally required. Therefore, the proposed modelling strategy and the major assumptions stated above might not be suitable for other structural systems like flat slabs or precast/prefabricated systems where the behaviour may be governed by punching or connection failures, respectively. Besides, the buildings considered in the present study are modern buildings which are designed using the present building codes (EN1992 for the concrete design [40] and EN1998 for the seismic detailing [41]). The modelling strategy proposed here might not be suitable for older structures built in the 1960s and 1970s (and earlier), which likely do not adhere to many of the detailing rules set by the present codes. Thus, they may experience unexpected failure modes such as joint failure, splicing or anchorage failure. In addition, the results obtained from the present study are mostly valid and applicable to buildings which are designed with some degree of seismic detailing. Thus, the findings should be treated carefully as they may not be directly translatable to building designs that consider no seismic design as the hierarchy of failures of the structural components might be somewhat different.

SAP2000 [42], which is a widely used structural analysis program by practitioners, was employed to perform all the computational simulations presented in this work. The applicability and accuracy of the adopted strategy were validated by comparing simulation predictions to selected experimental tests from the literature. The main findings of this validation exercise are shown in the following section (Sections 2.1, 2.2, and 2.3). Specific specimens and test campaigns have been chosen carefully to cover a wide range of scenarios, including 1) quasi-static tests of 2D frame systems without slabs [43], 2) dynamic tests of 2D frame systems without slabs [44], 3) dynamic tests of 3D frame systems including concrete slabs [45].

2.1. 2D-frame tests (without slabs) subjected to quasi-static load application

The test specimens were half-scaled RC beam-column subassemblies (2D frames without slabs) subjected to the removal of a central column [43]. Three specimens made of normal-strength concrete were selected: NSC-8, NSC-11, and NSC-13. The sole difference between these three specimens was the length of the beam, hence varying the span-to-depth ratio. The specimen NSC-8 is the shortest, with a beam clear span of 2 m, NSC-11 of 2.75 m, and NSC-13 of 3.25 m. The beam dimensions were 250 mm (height) x 150 mm (width). The subassembly's edge columns were restricted laterally and vertically. All three specimens had the same beam and column reinforcement configuration. The beam had 2 longitudinal bottom bars of diameter 12 mm along the whole beam; 3 top longitudinal bars of diameter 12 mm at the support and 2 top longitudinal bars of diameter 12 mm at the mid-span; and a shear reinforcement configuration of two-legged stirrups of 6 mm diameter spaced every 100 mm along the whole beam. The removed (middle) column had a dimension of 250 mm $\times$ 250 mm with 8 longitudinal bars of diameter 12 mm and three-legged stirrups of diameter 6 mm spaced every 100 mm. The edge columns had a dimension of 400 mm $\times$ 400 mm with 12 longitudinal bars of diameter 16 mm and four-legged stirrups of diameter 6 mm spaced every 100 mm. The stiffness of the lateral restraints (boundary conditions) was reported as 1×10^5 kN/m, and the same value was adopted in the numerical model reported in the present study.

The vertical load was applied over the central column using a displacement-controlled hydraulic jack (quasi-statically). Fig. 2b provides a schematic illustration of the SAP2000 model, including the boundary conditions adopted to mimic the actual test setup (Fig. 2a).

Fig. 3 below shows the calibration process where a systematic variation of the three main modelling parameters on specimen NSC-13 was performed: (a) concrete constitutive model (with and without confining effect); (b) number of fibre discretisation of the cross-section (throughout the depth of the member); and (c) the number of hinges per element length of the beam.

Fig. 3a indicates that the concrete confinement model produces steeper drops of vertical reactions after the first peak (i.e., when the concrete crushes at the end of the compressive arching action) at a displacement of around –100 mm and it also reduces slightly the final catenary capacities at around –700 mm vertical displacement. The influence is expected to be stronger for specimens with a shorter span-to-depth ratio where the arching action becomes more dominant. To ensure that accurate responses can be captured for general scenarios with various geometrical aspects, it is recommended to always include the effect of concrete confinement in the model. Fig. 3b shows a relatively mild influence of the fibre discretisation, but generally, about 6 to 10 fibres already provided consistent results. From these three investigated parameters, it is found that the influence of the number of hinges (Fig. 3c) is the strongest. A general trend can be observed: with fewer

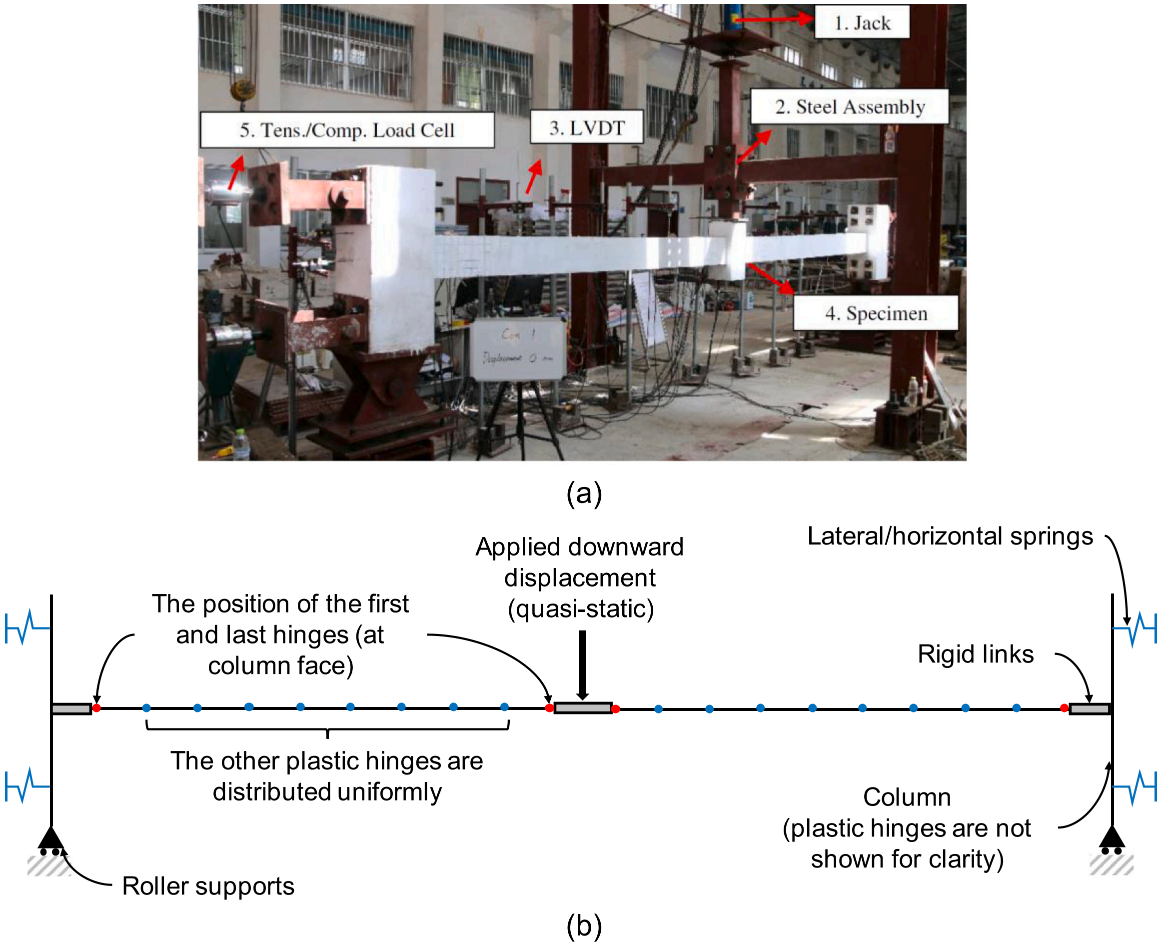

Fig. 2. (a) Test setup and instrumentation layout of the test campaign by Deng et al. [43]; (b) The adopted computational model. Image reproduced with permission of the rights holder (ASCE).

hinges, the peak load tends to be higher because this is analogous to having more uniform stress along the rebar. On the contrary, increasing the number of hinges led to an earlier fracture of the reinforcing bars as the tensile stress became more concentrated in shorter plastic hinge regions during the catenary state. Observing the responses in Fig. 3c, the best fit for the test results was achieved with 10 hinges, which became increasingly conservative as the number of hinges increased. Based on these analyses, it is recommended to use 10–20 hinges within one beam length to capture the fracture of the reinforcing bars realistically. This is consistent with previous observations by [31].

Fig. 4 compares the measured vs predicted responses of specimens NSC-8, NSC-11, and NSC-13 using the adopted modelling strategy (i.e., adopting the confined concrete model; 10 $\times$2 fibres for the cross-section discretisation; 10 hinges per element length).

Overall, Fig. 4 shows that the adopted computational model accurately predicted the vertical and horizontal responses of all specimens. The peak of the arching state, the transition from the arching to the catenary, and the peak of the catenary state were all correctly reproduced (these key points are indicated in Fig. 4a). However, a slight discrepancy can be observed in the first fracture of the longitudinal reinforcing bars that occurred earlier in the simulations (around the transition from arching to catenary). This can be explained by the fact that the adopted modelling strategy assumes a perfect bond condition (not accounting for the bond-slip phenomenon) that leads to a higher concentration of rebar tensile stress in a shorter region, leading to a slightly premature failure of the bars. A similar phenomenon was observed by Makoond et al. [46].

2.2. 2D-frame tests (without slabs) subjected to a dynamic column removal

In the original study [44], two half-scale specimens were tested: a cast-in-place concrete and a precast specimen. Only the cast-in-place specimen (specimen RC) was selected for validation here. The beam dimensions were 300 mm (height) x 200 mm (width), whereas the edge column was 350 $\times$ 350 mm. The specimen was pre-loaded with steel plates (weights) before performing the sudden column removal. In total, six different load stages were performed where the weights were incrementally increased for each stage to simulate different magnitudes of imposed loads. In this section, only the results of stages 2–5 will be presented as they are considered the most realistic range of loads to be encountered in practice (i.e., the 1st stage was performed with a very small load below the cracking point, whereas the 6th stage was very close to the collapse of the specimen where the behaviour was relatively unstable). Fig. 5 compares the measured and predicted responses in terms of vertical displacement vs. time at the location of the removed middle column.

Fig. 5 indicates that the predictions are in good agreement with the measured displacement responses for all load stages. Observing the dynamic motions, the numerical predictions seem to reach a state of equilibrium faster (i.e., the vibrations decayed in a shorter period). In contrast, the measured responses showed more waves of vibrations. One potential reason is the difference in the viscous damping in the system. As the damping values were not reported in the original test, we assumed a consistent viscous modal damping of 5 % consistently for all the load stages, which can be somewhat different in real tests [47].

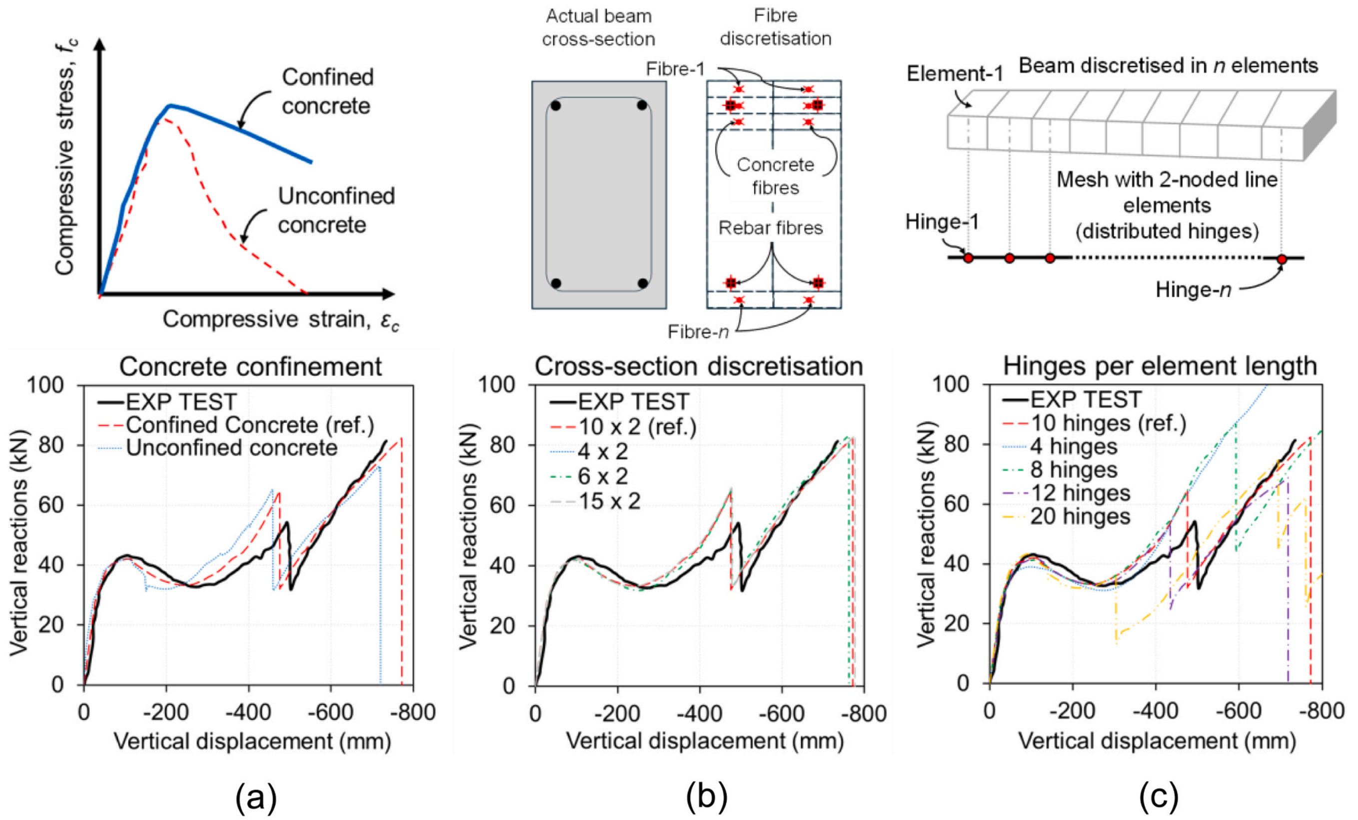

Fig. 3. Vertical load vs displacement response of specimen NSC-13 showing the influence of (a) the concrete confinement model, (b) fibre cross-section discretisation, (c) the number of hinges along the element length.

2.3. 3D-frame tests (with slabs) subjected to a dynamic column removal

The following study considers a more complex and realistic scenario where a 3D-frame specimen with slabs was subject to a sudden edge-column removal [45]. The ¼-scale specimen consisted of two complete bays: two spans in the longer direction and one span in the shorter one, supported on eight columns. The frame spans about 2.25 m in both directions (column's axis to axis), with a slab overhang of about 0.5 m representing the imposed loads from the parts of the floor system that were not included in the test specimen. Two different beam designs were used: interior beams with a dimension of 138 mm (height) x 80 mm (width) and perimeter beams of 112 mm × 80 mm. The column dimensions were square and were 170 mm × 170 mm. The slab thickness was 64 mm. The imposed loads were applied using external weights in the form of concrete blocks. The sudden column removal was performed using a special device designed to rotate (so-called ICRD, Instantaneous Column Removal Device), thereby releasing the axial forces after horizontal impact (Fig. 6a). Two specimens were tested under dynamic loading conditions: D-0.91 and D-1.16, but only D-0.91 will be discussed here as the latter behaved unstably, where the vertical deformation kept increasing even some hours after the test was terminated.

The two most used approaches for modelling the nonlinear behaviour of concrete slabs are 1) the grillage approach (Fig. 6b), where a slab is "substituted" by a series of orthogonally-arranged beams (line elements), and 2) the nonlinear-layered shell approach (Fig. 6c), where a slab is discretised into several thin layers along the height of the section. The nonlinear-layered shell adopted here follows a thick-plate response (Reissner/Mindlin) formulation which includes the effects of elastic transverse shear deformation. The in-plane interaction (normal and shear stresses) is modelled according to the Darwin-Pecknold concrete model [48]. Darwin-Pecknold (DP) model is a co-axially rotating smeared crack concrete model which can simulate an interaction between bending and shear. The interaction between transverse tensile strain and compressive strength in the perpendicular direction, the so-called "compression softening" effect, is accounted for based on the Modified Compression Field Theory (MCFT) of Vecchio and Collins [49]. The out-of-plane shear failure (punching) is not considered as the transverse shear response is modelled as elastic. This is deemed acceptable for the slab system adopted in the present study (not a flat slab one). The reinforcing bars inside the slab are modelled as a thin shell layer (single layer) with an equivalent thickness (i.e., the area of a single reinforcement bar divided by the spacing between two adjacent bars). For each layer, integration of the layer stresses is performed at standard 2 × 2 Gauss points to obtain the sectional slab forces (bending, twisting, and shear). Throughout the present study, the slab is consistently discretised into ten layers throughout the thickness. Unlike the typical (default) centroid-to-centroid connections, the connection between the slabs and the beams adopted in the present study was configured specifically so that the top surface of both elements is located at the same elevation (i.e., similar to a T-beam section). This was deliberately done in order to account for the bending stiffness of the beam-slab system more accurately.

Both approaches were used, and the resulting predictions are discussed in the following. Concerning the mesh size for the shell elements, generally, a mesh length between $L/10 - L/20$ is deemed acceptable to yield reliable predictions [50], with L as the centreline-to-centreline distance between two adjacent supports/columns. For this test series, L is about 2250 mm, and the average mesh size for the shells was taken as 100 mm (about $L/20$).

Fig. 7 compares the measured vs. predicted displacement responses obtained using the two approaches. For the grillage model, several plots are presented in Fig. 7 to demonstrate the influence of adopting different torsional stiffness modifiers on the predicted responses. Overall, it can be observed that the nonlinear shell approach predicted the slab

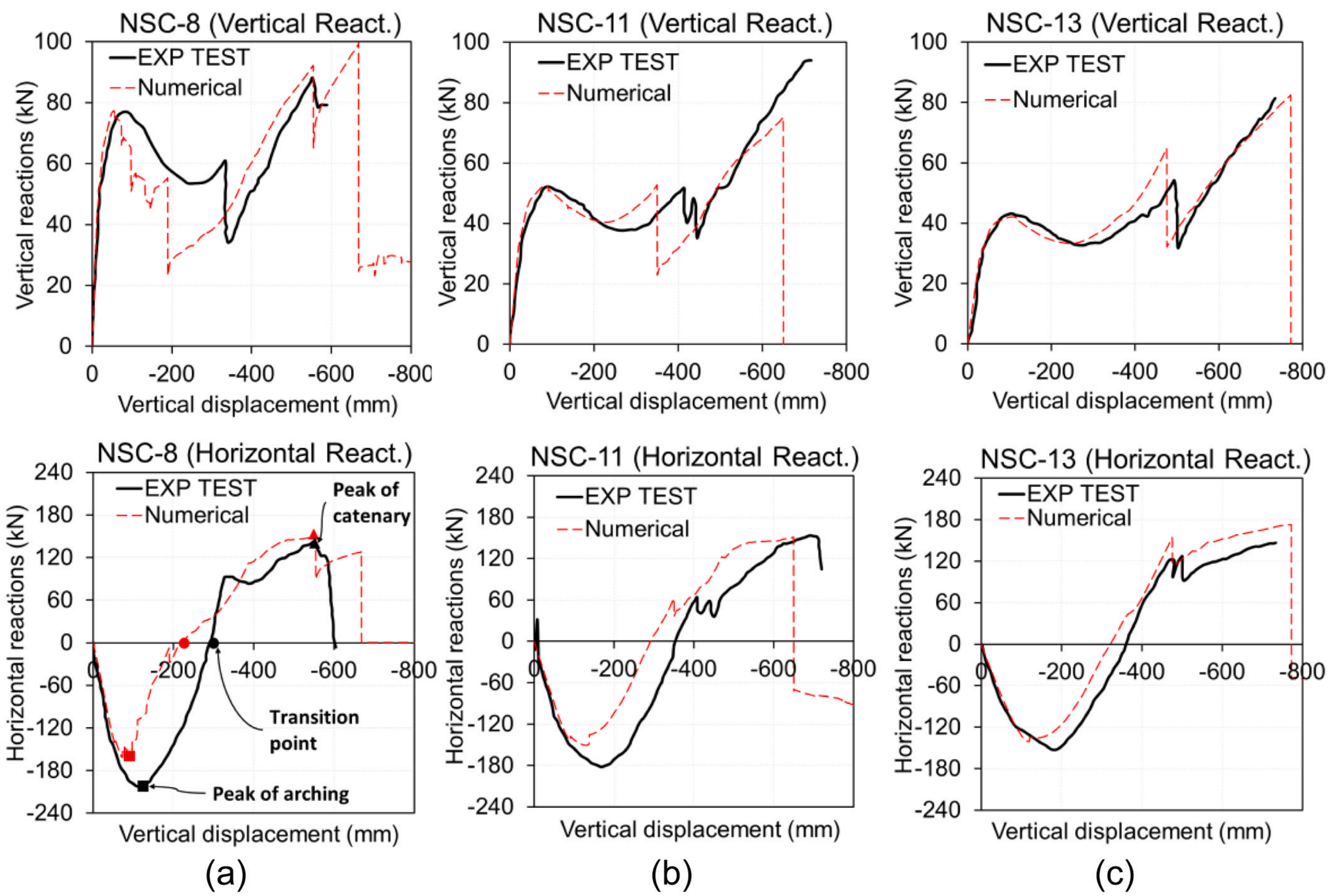

Fig. 4. Measured vs. predicted responses of specimens (a) NSC-8; (b) NSC-11; (c) NSC-13 subjected to quasi-static load (2D-frames without slabs).

responses well, particularly the residual displacement, with a slightly larger error in terms of the peak value. The grillage model's predictions are highly sensitive to the adopted torsional stiffness. The model with the smallest torsional stiffness modifier (0.08 of the uncracked torsional stiffness) best agreed with the measured response. In contrast, the grillage model without stiffness modifiers produced a much stiffer response. Considering this strong sensitivity, it is recommended to adopt the nonlinear-layered shell, as has been done for all the analyses described in the following sections.

2.4. Concluding remarks from the validation of the adopted modelling strategy

The results presented in Sections 2.1, 2.2, and 2.3 confirm that the adopted modelling strategy, combining distributed fibres for the frame elements and nonlinear-layered shells for the slabs, can produce accurate and reliable results with a reasonable computation time. Importantly, several modelling parameters must be chosen and calibrated carefully to ensure reliable results. For the line (frame) elements, the most important aspect is the number of hinges per element length. It is recommended to use between 10–20 hinges per element. Regarding the modelling of the slab, the predictions of the simplified grillage model are strongly affected by the reduction of torsional stiffness. Considering this strong sensitivity, it is recommended to adopt the nonlinear-layered shell with a mesh size of about $L/10$ – $L/20$. Having a properly calibrated model allows further objective evaluation of the robustness of a given structural system using various indexes. This aspect will be described in detail in Section 3.

3. Robustness index studies

The validated modelling strategy was further utilised to determine and compare the robustness indexes proposed by Khandelwal & El-Tawil [51], Bao et al. [52], Fallon et al. [53], and Fascetti et al. [54]. These four indexes are categorised as reserve-based deterministic indexes, and are deemed to be highly suitable for evaluating the effectiveness of design measures intended to improve load redistribution capacity [10]. These four indexes were selected because they vary broadly in terms of analysis procedure, and they also use different measures to express robustness. Table 1 summarises the four indexes, including their advantages and limitations. These indexes were used to measure the robustness of three hypothetical building designs: a) **Building A -** the control building (reference) with 5 × 5 bays as all the other buildings, 6 m span length and 3-storey height; b) **Building B** – with 10 m span length and 3-storey height (to evaluate the influence of span length); and c) **Building C** – 6 m span length and 6-storey height (to assess the influence of the number of stories or building height) whereas the floor layout was kept the same. The chosen span lengths of 6 and 10 m were selected to represent the practical lower- and upper-bound spans of typical RC buildings found in practice. Similarly, the 3 and 6-storey buildings represent a category of low-rise and mid-rise (bare) frame systems that can be generally found in practice (without the presence of lateral bracing or wall systems). These three buildings were seismically designed as ductility class medium (DCM) according to EN 1998 [41]. The structural robustness designs were performed according to the prescriptive tying rules of the UFC guidelines [6]. More detailed information on these three buildings (element dimensions and reinforcement configurations) is provided in Supplementary Material.

For each building, multiple notional column removals were

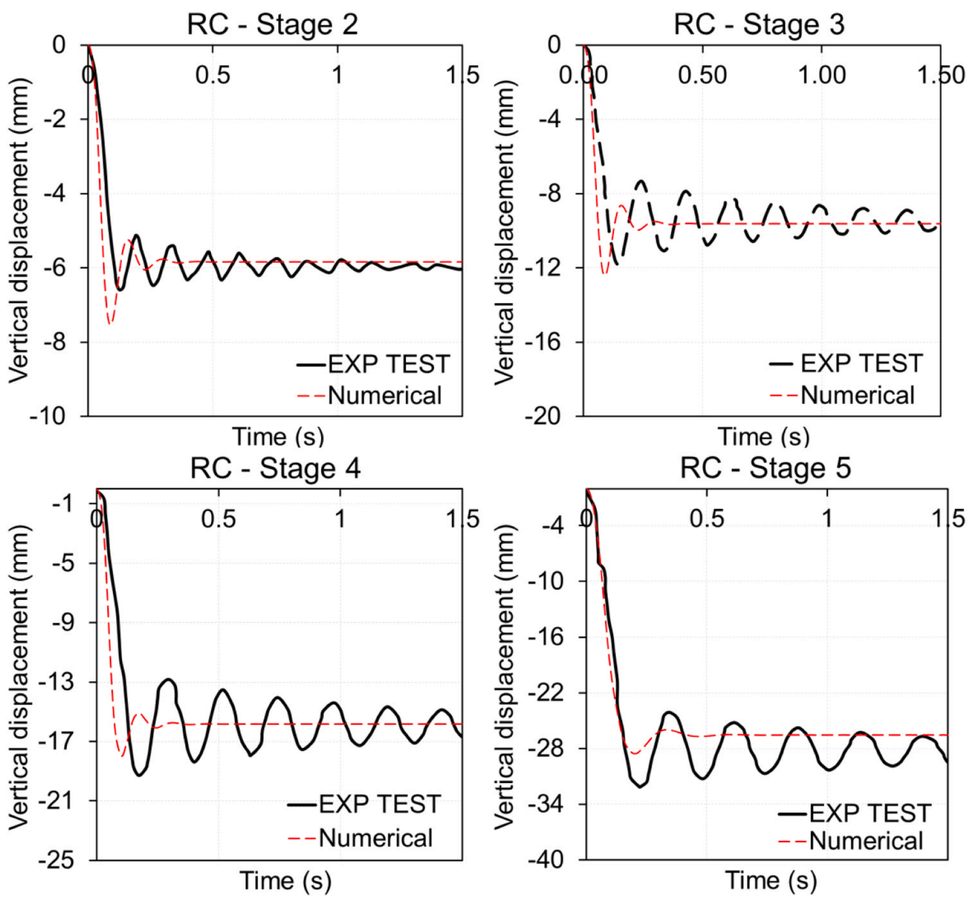

Fig. 5. Measured vs. predicted responses of specimens RC at four different load stages subjected to a sudden column removal (2D-frames without slabs) [44].

performed either individually or sequentially (depending on the robustness index procedure) according to a threat-independent approach. By taking advantage of the building symmetry and assuming that only the ground floor column removals are considered, there are six individual single-column removals to be investigated: one corner column removal, two edge column removals, and three internal column removals (refer to Fig. 8).

The following subsections will present an example of each index to demonstrate its implementation. For the sake of brevity, the demonstration described in the following sections is only for Building A, but the three buildings will be compared altogether and discussed in Section 3.5.

3.1. Index 1 by Khandelwal & El-Tawil [51]

In the original study of Khandelwal & El-Tawil [51], the authors proposed three alternative methods to analyse the structural robustness of a system: 1) nonlinear static bay pushdown, 2) nonlinear static global pushdown, and 3) incremental nonlinear dynamic analysis. In this paper, we adopted the first one as it is considered the most practical to perform. The bay pushdown shall be performed individually for each column location. It starts by deleting the column from the structural model (before the analysis), applying uniform accidental load combinations to the whole floor (in this study, we adopt 1.2DL+0.5LL according to the UFC accidental load combination [6]), and then gradually increasing the load only at the bay where the column is removed using a multiplier λ(1.2DL+0.5LL) until a collapse is triggered (Fig. 8). The value of imposed load (in LL) and superimposed dead load (in DL; in addition to the self-weight) used in the present study was 3 and 2 kN/m^2 respectively, that represent typical characteristic loads for office buildings according to EN 1991–1-1:2002 [55]. The robustness index is determined as the minimum λ value, considering all column removal scenarios. Fig. 9a shows the results of the bay pushdown for all six column removals of Building A. The last data point plotted in Fig. 9a was taken as the last converged step before a significant force, displacement, or energy error occurred. This represents the moment where no further system equilibrium could be achieved, indicating collapse initiation (either partially or totally).

As shown in Fig. 9a, the robustness index of Building A according to Index 1 equals 1.589, which corresponds to the removal of column Internal-1 (penultimate-internal column; Fig. 8). In general, all three internal removals consistently failed at a significantly lower vertical displacement when compared to the edge- or corner-column removal. A further investigation was done to identify the failure mode, and it was found consistently that for all scenarios involving the loss of an internal column, the failure was triggered due to the compression failure of the concrete of the surrounding columns (overload), leading to a brittle failure mode. In all removal locations, the load resistance increases (hardening response) after experiencing the first drop, indicating a possible force redistribution due to the formation of the catenary mechanism of the beams and the tensile membrane action of the slabs. Fig. 9b compares the force- and displacement-controlled procedures to perform the bay pushdown. The two procedures are in close agreement, where only a slight deviation occurs at the descending part of the curve (i.e., the force-controlled method shows a snap-through response). In the present study, all the analyses were performed consistently using the displacement-controlled procedure as it captures the whole structural response of the system, including the redistribution of loads between structural members, typically indicated by a decrease/drop of resistance.

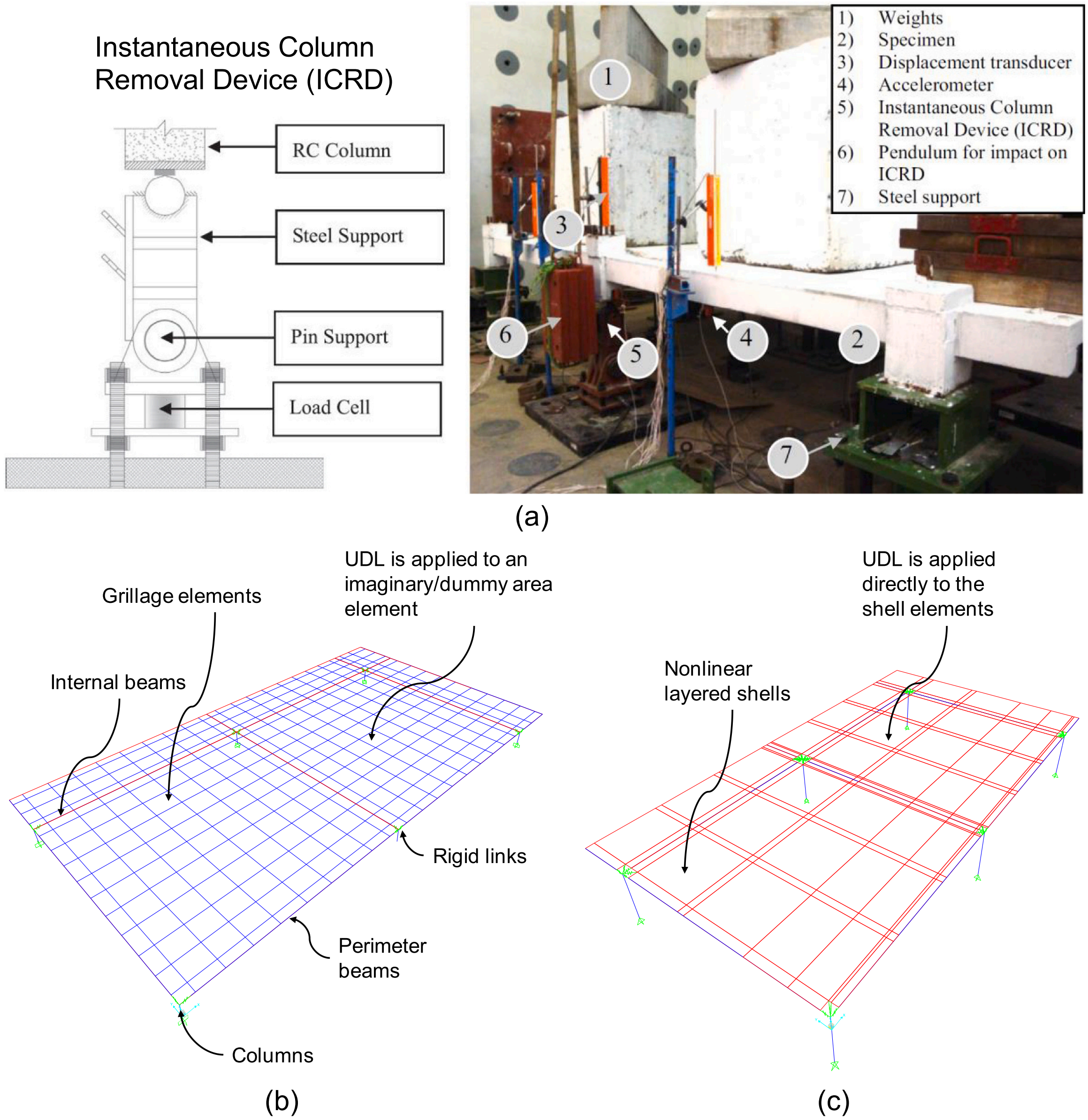

Fig. 6. (a) Test setup and important auxiliary components of the test campaign by Qian and Li [45]; two modelling approaches to simulate concrete slabs: (b) the simplified grillage model and (c) the nonlinear-layered shell model. Image reproduced with permission of the rights holder (Elsevier).

3.2. Index 2 by Bao et al. [52]

The robustness index proposed by Bao et al. [52] also adopts the local bay pushdown method (as Index 1), but it implicitly accounts for dynamic amplification using the energy conservation principle [56]. It is worth mentioning that the use of an energy-based approach to estimate the approximate dynamic resistance from the static response was first introduced by Izzuddin et al. [56], but the implementation of such a concept to quantify the robustness of a structural system was done by Bao et al. [52] - Index 2, as an improvement from the static index previously proposed by Khandelwal and El-Tawil [51] - Index 1. According to this principle, at any state, the external work done by the load (i.e., the load redistributed from the failed column and its corresponding displacement) is equivalent to the internal work done (i.e., the way the system redistributes the internal forces through straining actions). By assuming an SDOF idealisation, the pseudo-static response (approximating the real dynamic response) can be determined from the static-bay pushdown results in a straightforward manner using the following formulations:

$$\lambda_d(\Delta).\Delta = \int_0^{\Delta} \lambda_s(\Delta).d\Delta \tag{1}$$

$$\lambda_d(\Delta) = \frac{1}{\Delta}\int_0^{\Delta} \lambda_s(\Delta).d\Delta \tag{2}$$

where $\lambda_d(\Delta)$ is approximate dynamic capacity (pseudo-static resistance), Δ is the corresponding dynamic displacement, whereas the integral at the right-hand side of (Eq. 1) represents the area below the static pushdown curve, representing the potential energy absorbed by the system with $\lambda_s(\Delta)$ as the quasi-static resistance of the system.

Fig. 10 shows both the static bay pushdown and the pseudo-static responses for all six single-column removals of Building A. The maximum/peak load multiplier factor is plotted in the same figure. Fig. 10 shows that the λ factor, according to Index 2, varies from about 1.151 – 1.631, with the most critical scenario being the penultimate internal column (Internal-1), consistent with Index 1. The dynamic resistance of Internal-1 decreases from 1.589 in Index 1 to 1.151 in Index

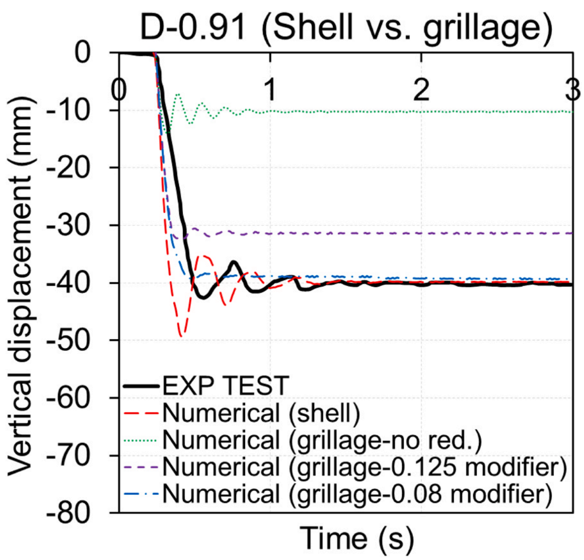

Fig. 7. Measured vs. predicted responses of specimen D-0.91 [45] subjected to sudden column removal (3D-frames with slabs).

2, which indicates the importance of accounting for the dynamic effect when determining the structural resistance. In this case, the design of Building A can be considered acceptable as the resistance against abnormal events for any single column removal is > 1.0.

In addition to obtaining the dynamic resistance, the energy-conservation principle can also be applied to estimate the system's dynamic amplification factor (DAF):

$$\mathbf{DAF} = \frac{\boldsymbol{\lambda}_{\mathbf{s}}(\boldsymbol{\Delta})}{\boldsymbol{\lambda}_{\mathbf{d}}(\boldsymbol{\Delta})} \tag{3}$$

These DAF values will be used when performing the global pushdown in Index 3. Fig. 11 shows the DAF values plotted as a function of the vertical displacement of all six columns of Building A. In the same figure, the DAF model proposed by Marchand et al. [57] (also adopted in [6]) for reinforced concrete structures is plotted to provide a benchmark. It is important to note that the model of Marchand et al. [57] was developed assuming a linear elastic, perfectly plastic (EPP) behaviour, which results in a continuous decrease (decay) in DAF as the plastic deformation increases. Fig. 11 indicates that the DAF obtained from the energy-conservation principle has a slightly different trend than the EPP model of Marchand et al. Particularly, the pattern of the curves obtained from the energy-conservation principle shows that the decreasing trend of the DAF reverses at a certain point and gradually increases until failure happens. This was possible due to the development of the catenary and tensile membrane actions at large deformation states that provide additional resistance to the system. In contrast, the EPP model does not account for this, which may underestimate the DAF at large displacement regions (unsafe design conditions). A consistent observation was recently reported by [58].

3.3. *Index 3 by Fallon et al. [53]*

Fallon et al. [53] proposed a robustness measure based on the ratio of the resistance provided by the damaged system relative to the undamaged resistance with all components intact. The index is referred to as the relative robustness index (RRI), and it is formulated as:

$$\mathbf{RRI} = \frac{\mathbf{L_{damaged}} - \mathbf{L_{design}}}{\mathbf{L_{intact}} - \mathbf{L_{design}}} = \frac{\frac{\mathbf{L_{damaged}}}{\mathbf{L_{design}}} - \mathbf{1}}{\frac{\mathbf{L_{intact}}}{\mathbf{L_{design}}} - \mathbf{1}} = \frac{\boldsymbol{\lambda}_{\mathbf{damaged}} - \mathbf{1}}{\boldsymbol{\lambda}_{\mathbf{undamaged}} - \mathbf{1}} \tag{4}$$

where $L_{damaged}$ represents the collapse load of the damaged structure, L_{design} represents the design load (in this case, accidental load combi-

Table 1
Summary of the four robustness indexes investigated in the present study [51–54].

Reference	Index formula/ expression	Advantages/ unique features	Disadvantages/ challenges
Index 1 [51]	$RI_1 = \frac{\text{Max static res.}}{\text{Design load}}$	• Simplest to perform; • Requires the least post-processing from the analysis results.	• Does not explicitly consider the dynamic effect; • Only applies for single-column removal scenario hence does not provide any indication of the critical propagation path.
Index 2 [52]	$RI_2 = \frac{\text{Max dynamic res.}}{\text{Design load}}$	• Requires the same analysis as Index 1; • Accounts for dynamic effect through energy-conservation principle (without requiring actual dynamic analyses).	• Only applies for single-column removal scenario hence does not provide any indication of the critical propagation path.
Index 3 [53]	$RI_3 = \frac{\lambda_{damaged} - 1}{\lambda_{undamaged} - 1}$	• Provides a measure of the reduction of global structural resistance for a given damage scenario relative to the undamaged state	• The resulting predictions are sensitively affected by the adopted dynamic amplification factor (DAF); • Only applicable for single-column removal scenario hence does not provide any indication of the critical propagation path.
Index 4 [54]	$RI_4 = \sum_{i=1}^{n_r} i * L_{n,cr}^{i}$	• It explicitly accounts for the dynamic effect (most realistic procedure); • The only index that allows identifying the critical propagation path through successive column removal procedures (multiple).	• Requires the most expensive computation time; • The index is not straightforward to interpret for evaluating a single building design (it requires another reference/ benchmark to be most useful).

Notes:
Max static res. = the maximum load that can be resisted by the structural system during the bay pushdown applied in a static manner;
Max dynamic res. = the maximum load that can be resisted by the structural system during the bay pushdown estimated using the pseudo-static approach (approximating dynamic analysis);
Design load = the design accidental load combination equivalent to 1.2DL + 0.5LL;
$\lambda_{damaged}$= the maximum load multiplier that can be resisted by the structural system during the global pushdown assuming a damaged system (removing the designated column);
$\lambda_{undamaged}$= the maximum load multiplier that can be resisted by the structural system during the global pushdown assuming an undamaged/intact system;
n_r = the number of columns to be removed to initiate progressive collapse;
i = the weighting factor based on the order of the column being removed (from 1 to n_r);
$L_{n,cr}$= the axial load multiplier for the critical column removed in each phase.

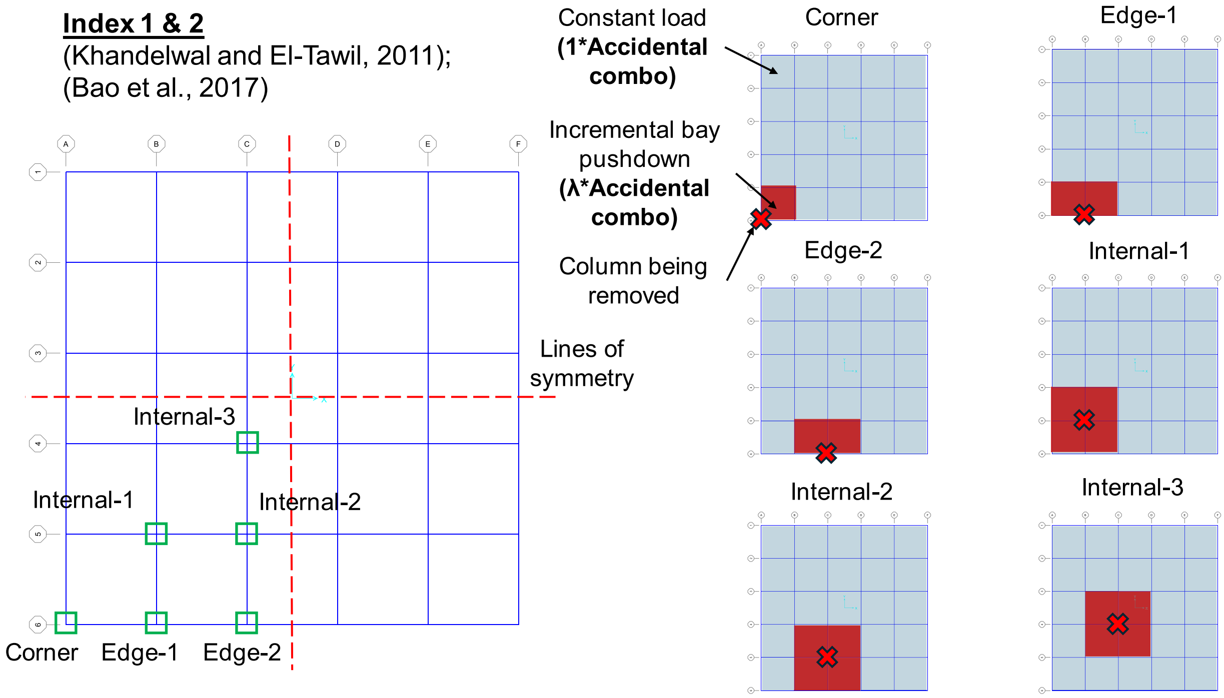

Fig. 8. Illustration of Indexes 1 & 2 procedure [51,52]: indicating the removed column locations and the affected bays where the local bay pushdowns are performed.

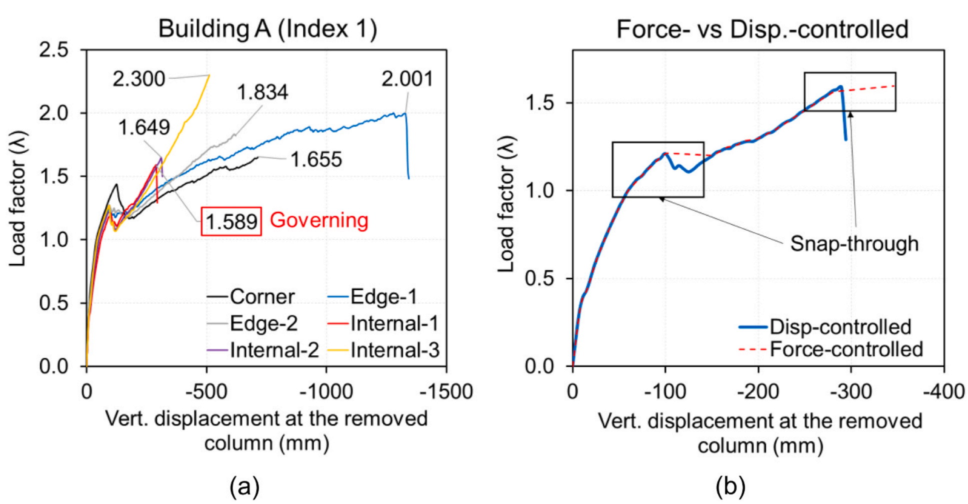

Fig. 9. (a) The results of the local bay pushdown of all investigated six-column locations of Building A (Index 1) – the λ values are indicated for each curve; (b) a comparison between force- vs displacement-controlled procedure to perform the local bay pushdown.

nation), L_{intact} represents the collapse load of the undamaged structure, $\lambda_{damaged}$ is the gravity load multiplier for the damaged structure (relative to the design load), and $\lambda_{undamaged}$ is the gravity load multiplier for the undamaged structure (relative to the design load). Global pushdown is used to measure the resistance of the structural system. The procedure is done by gradually increasing the uniformly distributed load in all bays but multiplying the accidental load combination with DAF for the bays affected by the column removal and a multiplier of 1.0 elsewhere (refer to Fig. 12). Fig. 13a summarises the RRI for all the six column-removal scenarios. The values of RRI for Building A vary between 0.265 (lowest – Internal 1) and 0.921 (highest – Corner). All values of RRI are always positive, which reflects that the structural system has sufficient resistance to fulfil the ALP check for accidental load combinations. The lowest value of RRI was observed for Internal-1 removal scenarios, which indicates that this scenario is the most critical for the system's integrity and is once again consistent with the previous indexes.

Fig. 13b demonstrates the sensitivity of the RRI to different adopted values for DAF for the Internal-1 scenario. Three variations of DAF were investigated: 1) one obtained from the energy-conservation principle (DAF=1.387); 2) Marchand et al. (DAF=1.302); 3) a linear elastic system (DAF = 2.0). It can be seen from Fig. 13b that the linear elastic model produces much lower RRI when compared to the other two models. This indicates that assuming DAF= 2.0 leads to a significant overestimation of the actual dynamic response of the system, leading to a very conservative result. The resulting RRI values from the energy-conservation principle and Marchand et al. are in reasonable agreement. These results suggest that selecting a realistic DAF is essential when determining the robustness index according to the Index 3 approach.

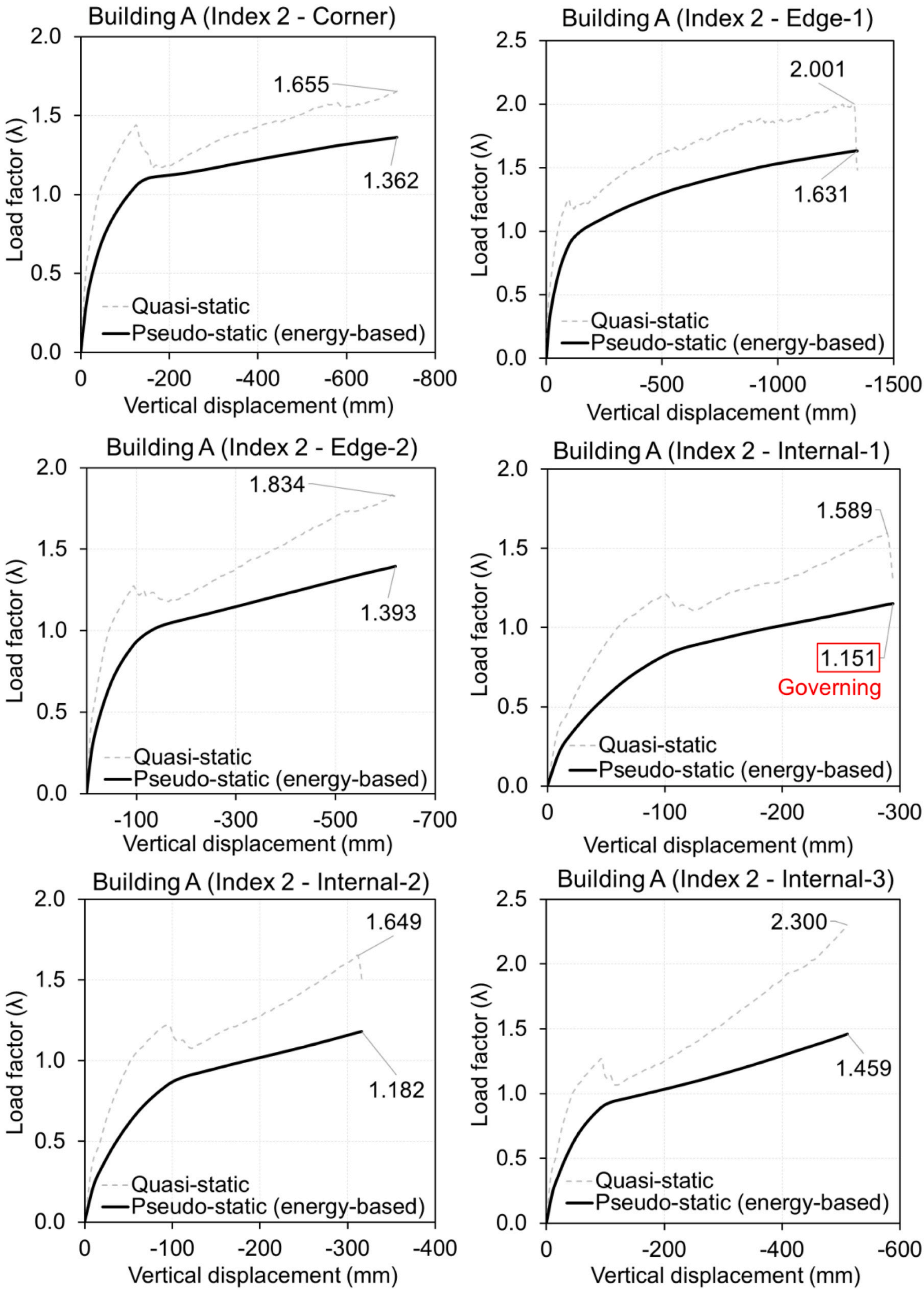

Fig. 10. Load factor vs. vertical displacement responses at the removed column location of six single-column removals of Building A (static and pseudo-static responses) – Index 2 [52].

3.4. Index 4 by Fascetti et al. [54]

The fourth index combines dynamic column removal and nonlinear static pushdown at the removed column location. Unlike the other indexes, Index 4 requires performing sequential dynamic removal by gradually removing the critical columns in the system until collapse occurs. Thus, the index does not only provide a measure of the load the system can resist before the collapse but also reveals the critical path

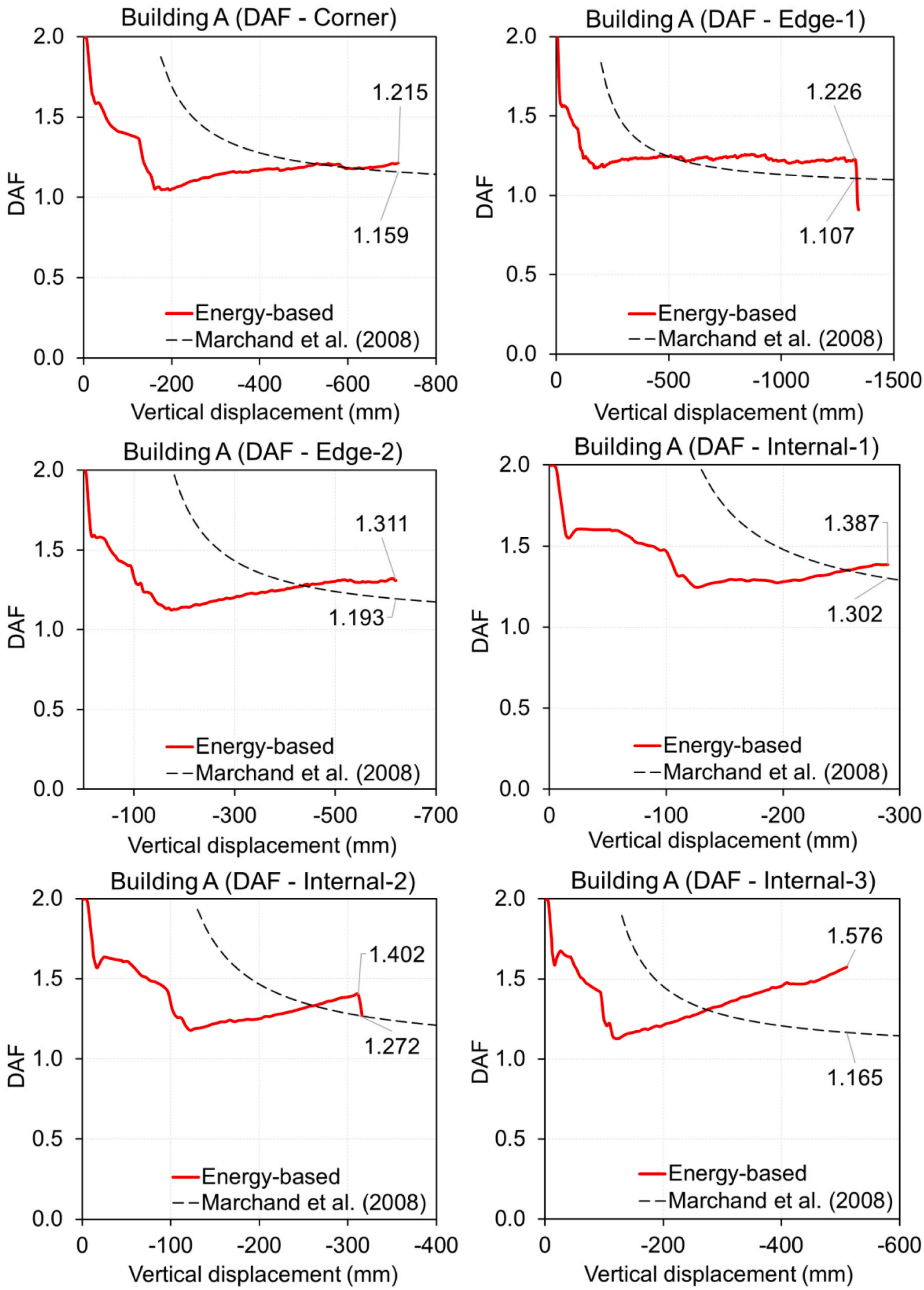

Fig. 11. Dynamic amplification factor (DAF) for six single-column removals of Building A obtained using pseudo-static analysis vs. Marchand et al. model.

where the collapse would likely initiate and propagate. Fig. 14 illustrates a single cycle to obtain Index 4:

1. The cycle starts by imposing uniform pushdown everywhere in the building according to the accidental load combination.
2. Then, a specific column/support is dynamically removed from the system.
3. Perform a check to determine whether a new state of equilibrium is possible.
4. If no equilibrium is achieved, then the process is terminated.

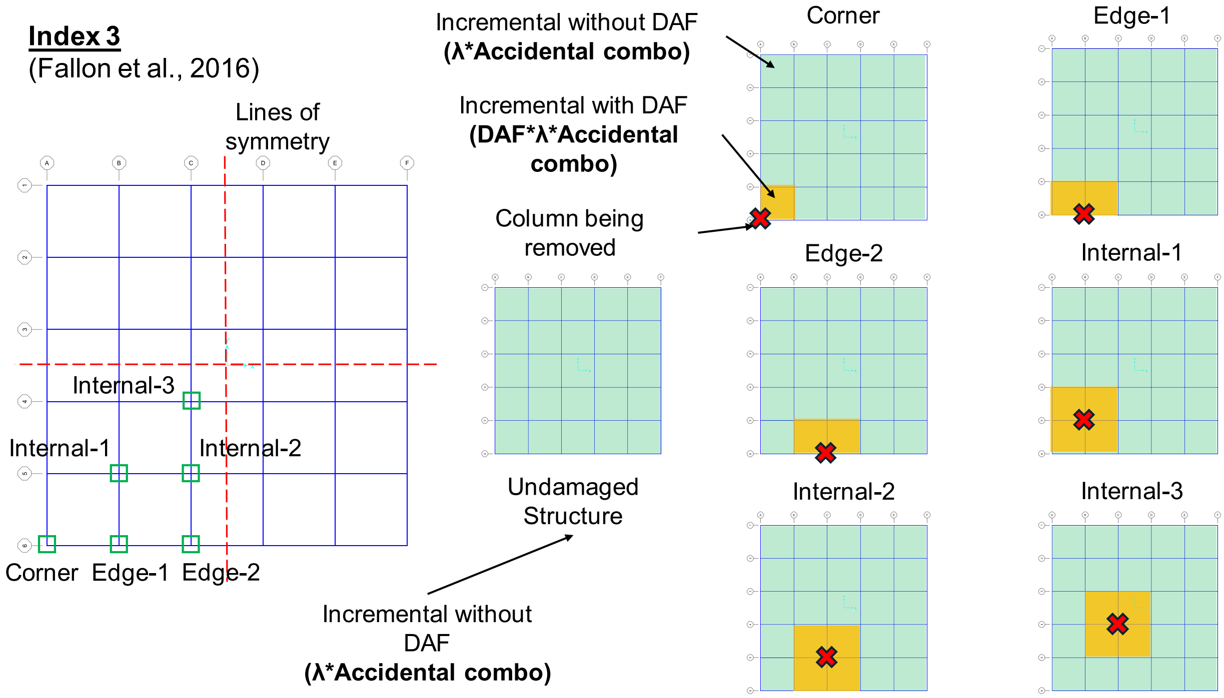

Fig. 12. Illustration of Index 3 procedure [53]: indicating the removed column locations and the load amplification factor for the affected and non-affected bays to perform the global pushdown analysis.

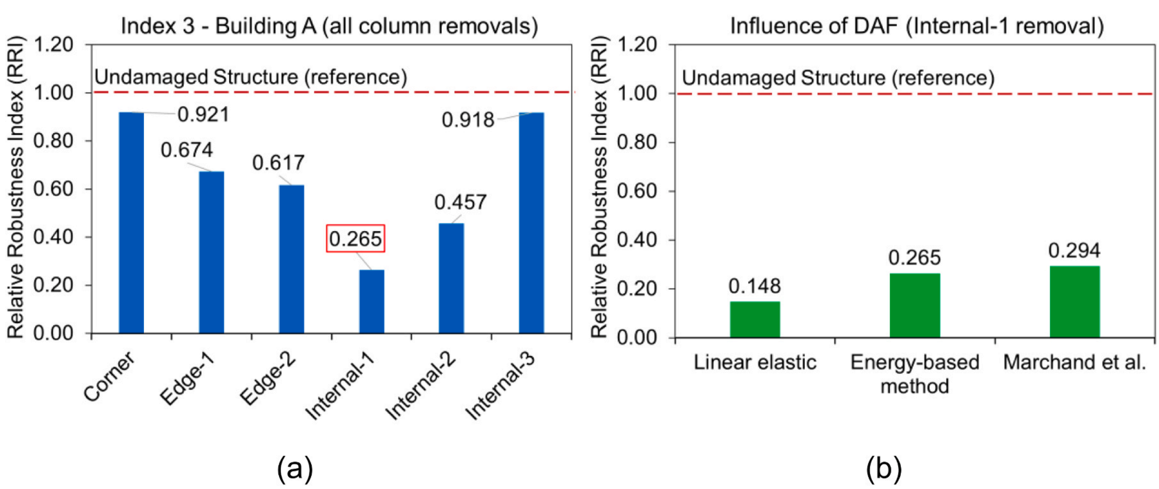

Fig. 13. (a) Relative robustness index (RRI) of all six column removals of Building A – Index 3; (b) The influence of the dynamic increase factor (DAF) on RRI.

5. If equilibrium is achieved, the process continues by performing a nonlinear static pushdown, applied at the node where the corresponding column was removed until collapse takes place.
6. Redo Steps 1-5 by removing the (adjacent) critical columns successively until no equilibrium is achieved when performing the dynamic removal. For more detailed information regarding the procedure, refer to Fascetti et al. [54].

It is important to mention that, for each cycle described in steps 1–6 above, a new (updated) numerical model is required as the critical element identified in step 6 must be removed manually from the corresponding model before proceeding to the next cycle/phase.

Figs. 15–17 show the three successive column removal phases performed to obtain Index 4 for Building A. Fig. 15 (left) indicates that all six single-column removal scenarios performed in Phase 1 can achieve a new equilibrium state. This suggests that the system fulfils the robustness requirement prescribed by the building codes according to the ALP (alternative load path) check. This conclusion is consistent with all the three previous indexes where $\lambda > 1.0$ for Indexes 1 and 2, and RRI ≥ 0 for Index 3. Fig. 15 (right) shows the nonlinear static pushdown performed after the dynamic removal, and the plots suggest that column Edge-1 produced the lowest load factor (λ), equal to 1.062. Thus, the first cycle concludes that Edge-1 will likely be the first column where the failure will be initiated. Interestingly, this conclusion is different from the other indexes where the critical scenario was consistently predicted as Internal-1. This is because the incremental load applied after the dynamic analysis in Index 4 is applied as a point load at the joint where the column is removed instead of a uniformly distributed load as in the previous three indexes. In Fig. 16 (Phase 2), three possible combinations of two-column removals were checked (adjacent to Edge-1): 1) Edge-1 + Corner; 2) Edge-1 + Internal-1; 3) Edge-1 + Edge-2. Fig. 16 shows that all three scenarios achieved a new state of equilibrium, and the

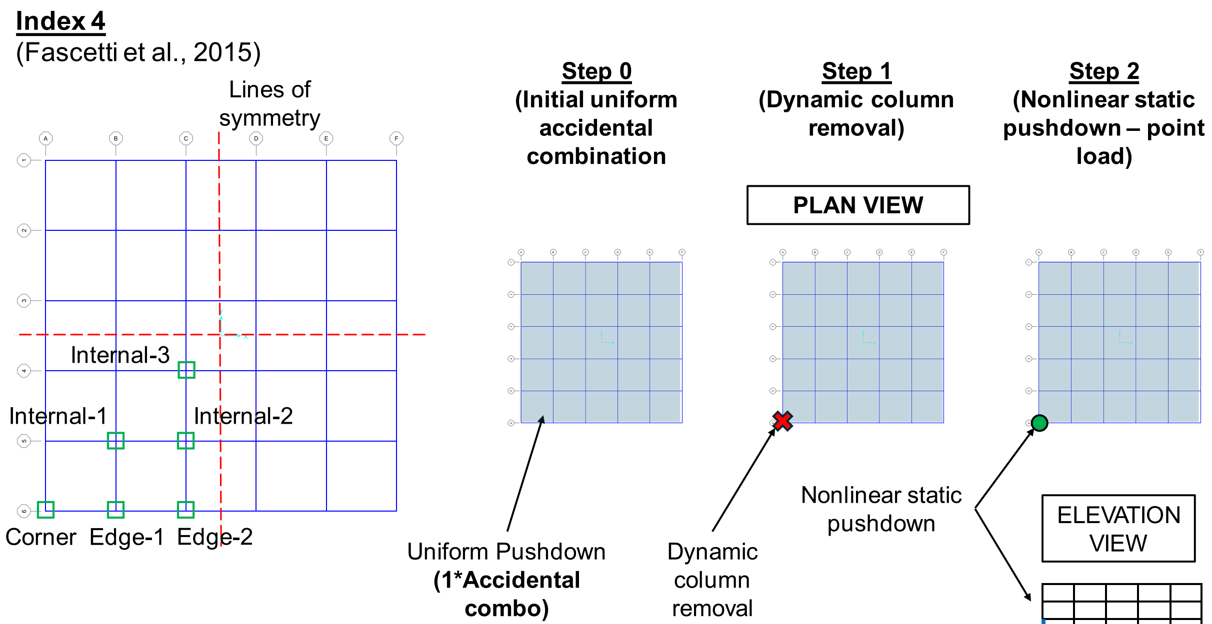

Fig. 14. Illustration of the procedure applied for a cycle of Index 4 (Fascetti et al.[54]).

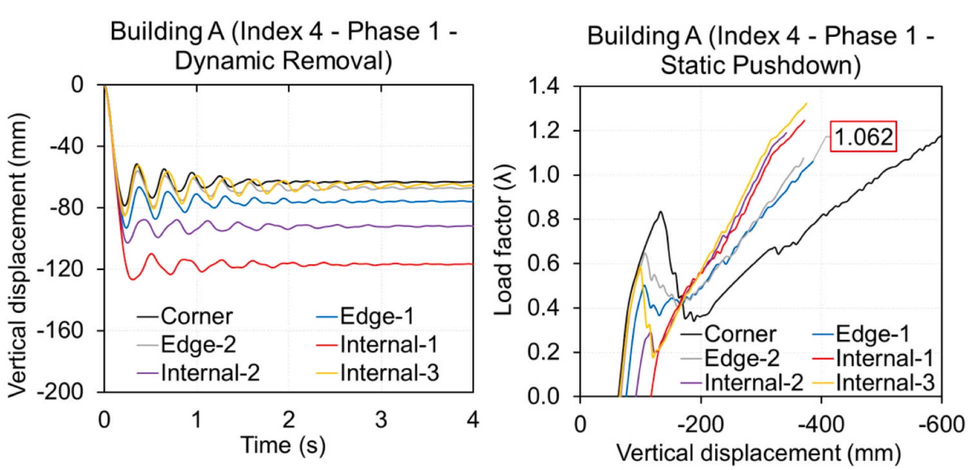

Fig. 15. Phase 1 of Index 4 [54] applied to Building A.

subsequent critical column was identified as Corner (lowest $\lambda = 0.836$).

Fig. 17 shows the procedure's final phase (Phase 3), where the system collapses after removing the third column (either Internal-1 or another Edge-1 column). This indicates that Building A can only sustain two-column removals and that it fails after the third. Based on the mathematical formula proposed by Fascetti et al. [54], the robustness index for Building A can be calculated as follows:

$$\boldsymbol{RI} = \sum_{i=1}^{n_r} \boldsymbol{i} * \boldsymbol{L}_{n,cr}^{i} = (\mathbf{1}) * \lambda_1 + (\mathbf{2}) * \lambda_2 = (\mathbf{1})\mathbf{1.062} + (\mathbf{2})\mathbf{0.836} = \mathbf{2.735} \tag{5}$$

where n_r indicates the total number of columns being removed before collapse is triggered, i indicates a weighting factor depending on the order of the column removal and $L_{n,cr}^{i}$ indicates the load factor (λ) the corresponding column can withstand under the nonlinear static pushdown. Using the equation above, we obtain a robustness index of Building A equals 2.735. This index cannot be interpreted individually, as the number alone might not provide any meaningful information. However, the index is useful for comparing different building designs or structural systems where a lower value indicates lower robustness and vice versa, as will be discussed in the next section.

3.5. Comparison of the four robustness indexes applied to Buildings A, B, and C

In this section, the summary of all four indexes applied to Buildings A, B, and C will be presented, and a systematic discussion will be provided to evaluate 1) the consistency between indexes and 2) the influence of building characteristics (span length and number of stories) on its structural robustness.

Fig. 18 shows the robustness index for individual column locations calculated according to Indexes 1–3. It is essential to mention that Index 4 is not included in Fig. 18 because it cannot be expressed for individual column loss scenario but instead as a single global (system) index. Fig. 18 indicates that in all three buildings, the indexes suggest that the critical scenario is the loss of the Internal-1 penultimate-internal column, except for Index 1 – Building C where Internal-2 is governing. This can be explained as the load that must be redistributed at the internal column is typically higher due to the corresponding column's tributary area, making it more critical than the edge or corner column. Besides,

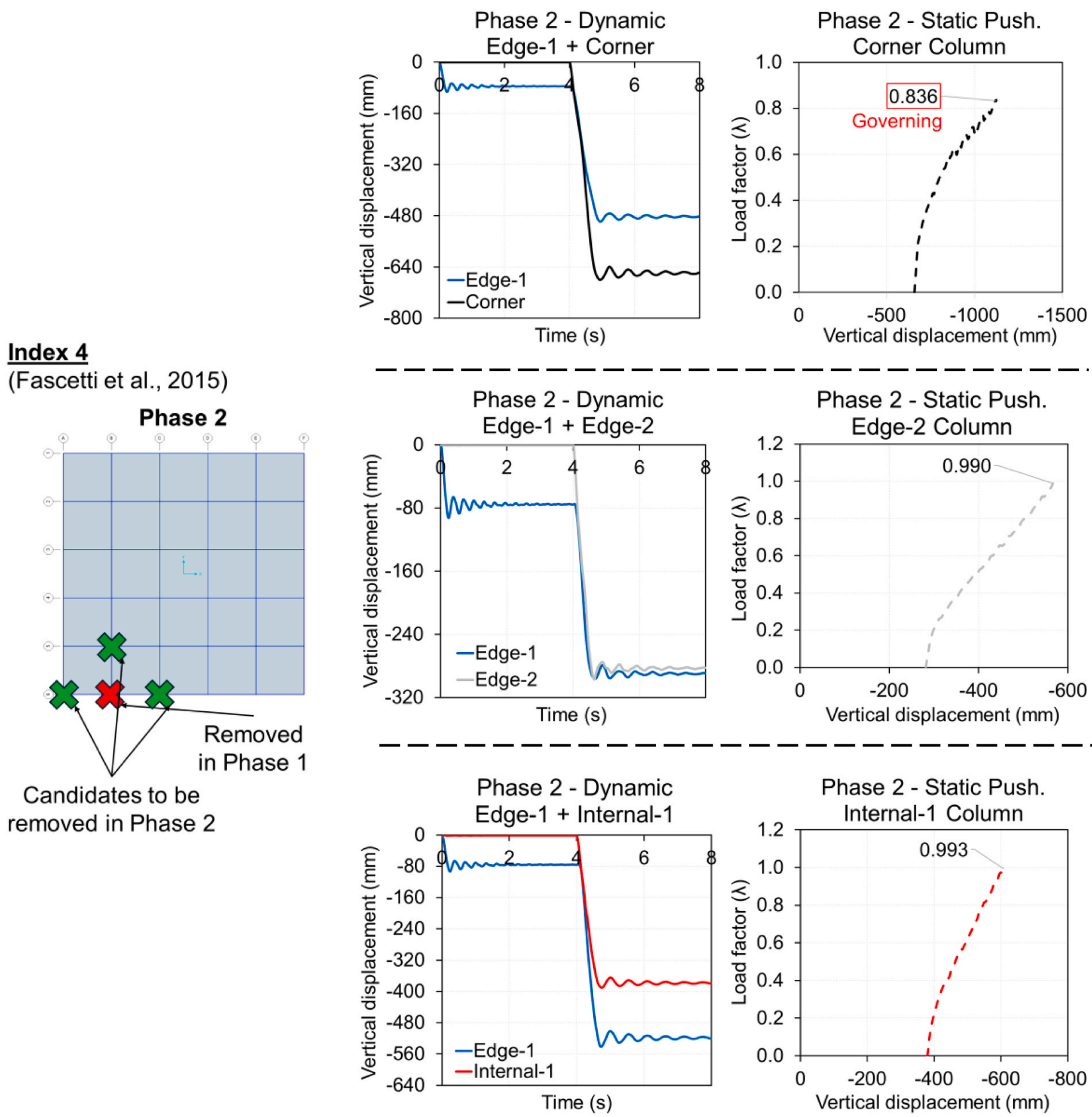

Fig. 16. Phase 2 of Index 4 [54] applied to Building A.

when comparing Internal-1, 2, and 3, Internal-1 is located closest to both the free edges of the building where the lateral stiffness provided by the system is lowest, leading to the weaker development of both catenary actions of the beams and tensile membrane actions of the slabs [59,60]. Another observation suggests that the difference between the robustness index for Internal-1 and Internal-2 is always very narrow. This is relevant for protective design as the two columns are located next to each other and could be damaged simultaneously during an extreme event such as a blast or a fire.

In Fig. 19, the final robustness indexes (Index 1–4) for all three buildings are summarised. According to Indexes 1–3, it can be observed that Building B, with a longer span, is always the least robust. Building B scored 1.081 for Index 2, indicating that the system is close to not fulfilling the ALP requirement for a single-column loss (with $\lambda < 1.0$). This is consistent with Index 3, which gave Building B a score of 0.146, which is very close to 0 (not fulfilled if RRI < 0). Buildings A and C produced very similar scores for Indexes 1–3. Regarding Index 4, a slightly different pattern can be observed. The three buildings survived with at least two column removals, and they collapsed after the third column was successively removed. However, the critical path is different: Building A = Edge −1 -> Corner; Building B = Internal −1 -> Internal-2; Building C = Internal-1 -> Edge-1. One observation that can be made is that for Building B, where the span is longer, the critical path starts and propagates through the inner parts of the building, where the tributary area is the largest (dominated by gravity loads). On the other hand, in Buildings A and C, with a 6 m span, the critical path mainly crosses the perimeter and corner parts of the building. Comparing Buildings A and C, it can be seen that Building A scored 2.735, whereas Building C scored 1.909. This can be potentially caused by the fact that with more floors, Building C is subjected to higher unbalanced moments when the local pushdown is applied, hence scoring lower for Index 4.

Evaluating a system using multiple robustness indexes proved more valuable, providing a more complete picture of system performance than relying solely on a single index. Indexes 1 and 2 are the most straightforward and simple to apply, and they provide a direct measure of how robust the system is in resisting the prescribed accidental load

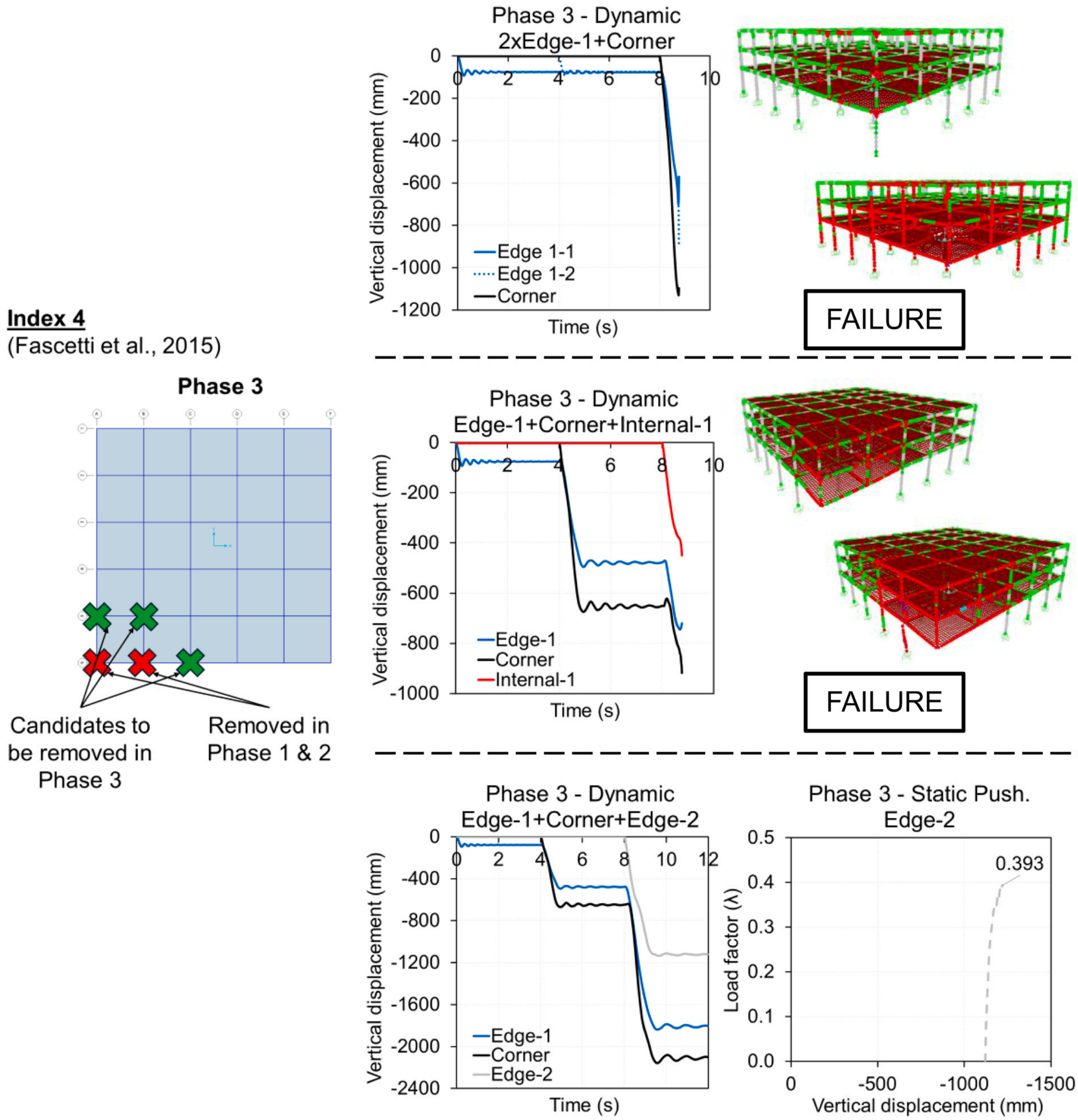

Fig. 17. Phase 3 of Index 4 [54] applied to Building A.

combination under a particular damaged state. They can also be used to identify the most critical column loss scenario (spatially) for a given building design. Index 3 compares the resistance of damaged and undamaged states of a system. As such, it provides a quantitative measure of how sensitive a system is (how much the global resistance is affected) to different considered initial damage scenarios. Although Index 4 is considered the most time-consuming as it requires successive dynamic column removals, it may reveal useful information about the behaviour of the building, including the critical path and the maximum number of columns being removed/damaged before global stability is lost. Such information cannot be obtained from the other three indexes, and it is more associated with the path a building would follow in case of disproportionate collapse.

Besides, the data extracted in one index can be used to compute others. For instance, Index 2 can be obtained simply by performing a post-processing of the static load-deformation response extracted for Index 1. Besides, DAF obtained from Index 2 can be used when performing the global pushdown in Index 3. This allows users to obtain several indexes by performing a limited number of computational simulations. Considering the effort and computation time required to perform the analysis and the usefulness of the index, it can be concluded that Index 2 is the most practical to use. It requires only a nonlinear static pushdown that is less time-consuming than the dynamic analysis, yet it indirectly accounts for the dynamic effect through the energy-based principle. In the following section, the potential usefulness of Index 2 to two specific applications is presented.

4. Potential application of robustness index

In this section, two practical examples are presented to further demonstrate the potential applications of Index 2 as a decision-making tool for practising engineers. Section 4.1 shows how the robustness index can be linked to the damage state (condition) of individual structural components. In Section 4.2, a systematic comparison between

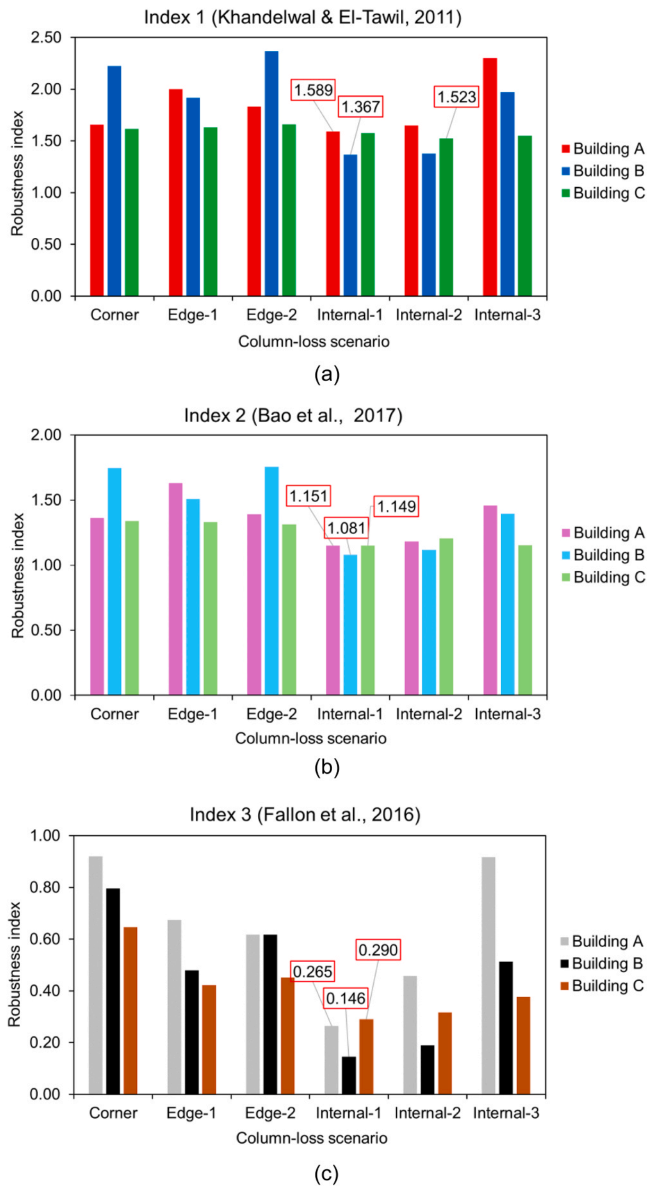

Fig. 18. The robustness index for each (individual) column-loss scenario of Buildings A, B, and C for (a) Index 1 [51], (b) Index 2 [52], and (c) Index 3 [53].

various retrofitting schemes was performed by utilising the index.

4.1. *Relating the robustness index to the damage state of the structural components*

All four indexes used in the previous section have provided different measures of the system's robustness. However, they did not explicitly indicate the level of damage suffered by individual components involved during the development of the alternative load paths. To provide such information, further post-processing can be done by linking the robustness index (global system response) to the elements' damage state (strain, stress, or rotation). For a demonstration, the damage state classification proposed by Parisi et al. [61] will be adopted. The classification consists of five limit states:

1. LS1 (slight damage): represented by minor concrete cracking or steel yielding in critical portions of beams located in floor areas above the removed column. The threshold is controlled by the strain in the concrete cover and the longitudinal reinforcement bars.
2. LS2 (moderate damage): moderate cracking of concrete cover in the affected beams, assumed to be controlled by the beams' rotation.
3. LS3 (significant damage): concrete spalling and concrete core's cracking that is controlled by the maximum strain of the beams' concrete cover and core.
4. LS4 (extensive damage): crushing of concrete core controlled by the maximum strain experienced by the concrete core.
5. LS5 (progressive collapse): a state where the partial or total collapse of the building occurs, controlled by either the fracture of the beams' longitudinal bars or a rotation limit of the beam.

This application is illustrated using the pseudo-static curve obtained using Index 2 for Internal-1 removal from Building A. Two specific beams were assessed: Beam-1 connecting Internal-1 and Edge-1 (Fig. 20a), and Beam-2 connecting Internal-1 and Internal-2 (Fig. 20b). Both beams are located at the ground floor level). Fig. 20 correlates the global pseudo-static curve (Index 2) with the damage state of the two investigated beams. The accidental load requirement (λ=1) is also plotted in the same graph.

Two main observations could be made from Fig. 20: 1) either beam has not reached LS5, which indicates that global failure occurs before the beams reach their limit of catenary state, suggesting that the failure of the columns governs; 2) Both beams are severely damaged at λ= 1, with Beam-1 trespassing LS3 and Beam-2 already trespassing LS4. This indicates that extensive repair would be necessary if such an extreme scenario occurs. Linking the robustness index to the damage state provides more complete information about the (global) system's state with the local damage of the engaged structural components. Knowing the damaged state of individual components, further post-processing could even be made to estimate the cost required for performing repair and replacement, for instance, according to FEMA P-58 methodology [62]. These costs can be used to estimate the consequences associated to the occurrence of different possible failure scenarios. Combining such consequences with estimates of the probability of occurrence of the scenarios would enable a holistic risk assessment of the structural system to be carried out.

In addition to this, combining the robustness index and the damage state, as shown above, can also be useful to assist the decision-making process during the design stage (even before any extreme event takes place). For example, the information gathered from such analyses can be utilised to decide whether we need to redesign some elements in our buildings in order to ensure an acceptable damage limit state (within a performance-based approach). In such a way, we can ensure that alternative load paths can be developed effectively while also limiting the damage to the surrounding elements when local failures take place.

4.2. *Evaluating and comparing the performance of various design/retrofitting solutions*

Another potential use of Index 2 is to systematically evaluate and compare several design/retrofitting solutions for a specific building/column-loss scenario. For instance, from the previous robustness evaluation of Building A, it was observed that the Internal-1 scenario always governs. Although it fulfils the accidental load requirement, the margin of safety is minimal. A further investigation was performed using Index 2 to compare various retrofitting solutions for the Internal-1 scenario. In particular, three solutions were investigated involving strengthening different building components: 1) strengthening the catenary actions of the beams by attaching a 3 mm layer of additional steel plate at the bottom surface of the beam (steel material S355); 2) strengthening the tensile membrane actions of the slabs by adding a rebar mesh made of Φ10 mm bars, spaced every 100 mm, at the bottom surface of the slabs; 3) increasing the resistance of the column against compressive loads by increasing the concrete strength from C30/37 to C50/60. For an existing building, solution 3 might not be possible, but an equivalent solution can be adopted, for instance, by using column jacketing to increase the cross-

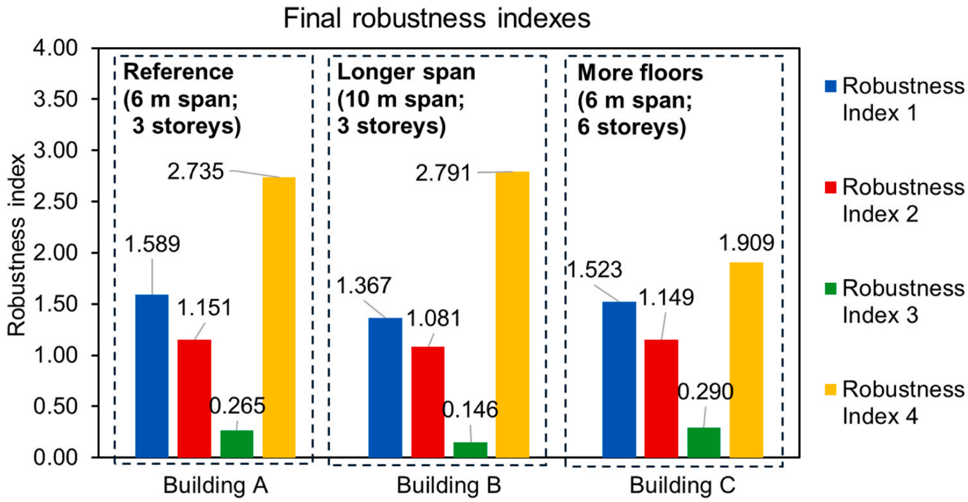

Fig. 19. Summary of the robustness index of Buildings A, B, and C.

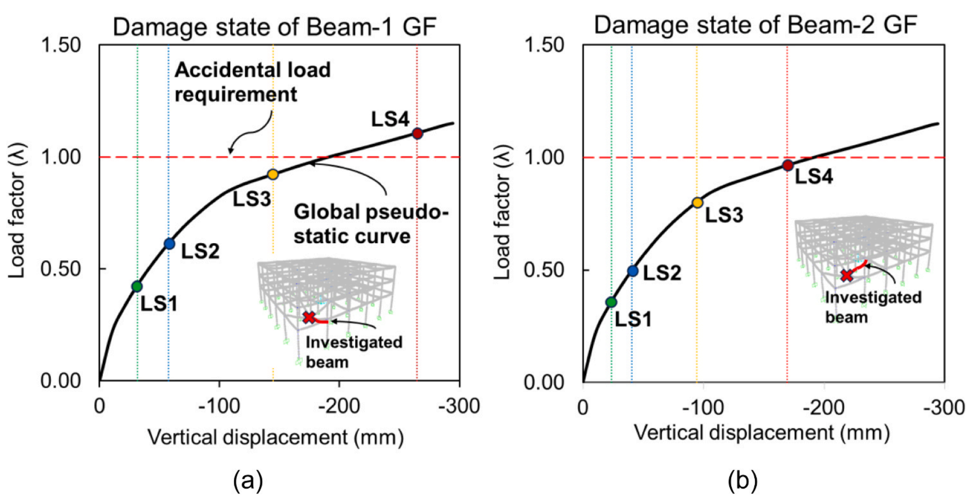

Fig. 20. Correlation of the global pseudo-static curve (Index 2) for the removal of column Internal-1 (Building A) to the damage state of (a) Beam-1 connecting columns Internal-1 and Edge-1; (b) Beam-2 connecting columns Internal-1 and Internal-2 (both at GF level).

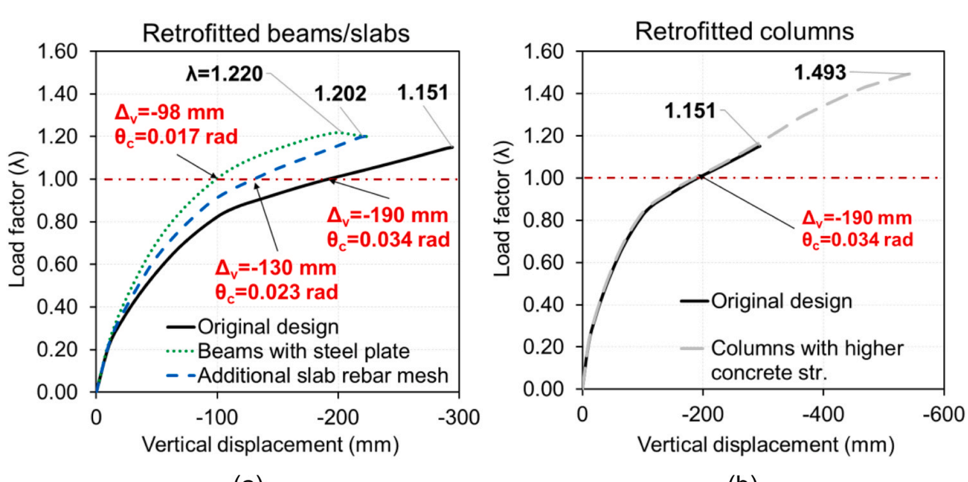

Fig. 21. Systematic evaluation of various design/retrofitting solutions using Index 2 for Internal-1 removal of Building A: (a) original design vs. strengthening of beams and slabs; (b) original design vs. strengthening of columns.

sectional area or introducing more confinement with FRP (fibre-reinforced polymer) to increase the confined concrete compressive strength.

In all these solutions, only structural elements directly affected by the removal of Internal-1 were strengthened. Fig. 21a compares the pseudo-static curve of the original design with solutions 1 and 2, whereas Fig. 21b compares the original design with solution 3. Fig. 21a indicates that solutions 1 and 2 achieved lower vertical deformation (Δ_v) at the level of load corresponding to the accidental load combination, leading to less system damage. Adding the steel plate to the beam reduces the chord rotation (θ_c) from 0.034 rad (original design) to 0.017 rad, whereas the additional slab mesh to 0.023 rad. However, it is interesting to note that the peak resistance ($\lambda_{\max}$) does not substantially increase for either solution (within the range of 1.1–1.2). This, once again, justifies that the failure of the columns initiates the global system failure. Hence, full activation of neither the catenary of the beams nor the tensile membrane of the slabs can be achieved. On the other hand, Fig. 21b shows that increasing the column compressive strength substantially increases the $\lambda_{\max}$ from 1.151 (original design) to 1.493, an increase of about 30 %. However, such a solution does not improve the performance of adjacent beams at $\lambda = 1$ as the new design experiences the same chord rotation as the original design (i.e., the adjacent beams experience the same magnitude/level of damages). An optimum (cost-effective) solution can be achieved by mixing strengthening solutions for different members according to the desired performance objectives. It is important to note that the two examples presented in this section were performed using only one robustness index (Index 2). More detailed assessment and retrofitting evaluations should be, in reality, performed with multiple indexes as they may provide different yet valuable insights (as discussed in Section 3). For instance, if retrofitting was only done locally in one part of the building, the distribution of element resistance in the system would change, resulting in potentially different critical paths. In this case, re-evaluation of the retrofitted system using Index 4 can be beneficial. Nevertheless, the corresponding example strongly demonstrates that the robustness index is a useful tool that can be used by practising engineers to systematically explore, compare, and eventually decide the optimum design/retrofitting solution for a given case.

5. Conclusions

This study proposes a practical methodology to evaluate and quantify structural robustness of RC buildings by combining an efficient modelling strategy and suitable robustness indexes. The modelling strategy explicitly accounts for nonlinear materials and geometry under large deformations, dynamic effects, and 3D-framing effects, including the contribution of the floor slabs. The proposed model was then used to quantify structural robustness using four different indexes for three hypothetical building designs. Finally, two practical applications are presented to demonstrate the potential of combining the proposed modelling strategy with one of the selected robustness indexes as an effective decision-making tool for practising engineers.

The main findings of the present study are summarised below:

- To model the beam and column elements, the use of a distributed fibre hinge approach (instead of lumped hinges) is recommended as it can realistically capture the spread of plasticity (yielding of the reinforcement bars) along the members during the catenary state. The most influential parameter that was found to affect the response is the amount of discretisation along the element length. For cast-in-place RC beams and columns (studied in this work), it is recommended to use at least 10-20 hinges per length to capture reliable behaviour during catenary stages.
- To account for the contribution of the floor slabs, two modelling alternatives were explored: a simplified grillage model and a nonlinear layered shell. The accuracy of the equivalent beam (grillage) model was found to depend significantly on the adopted torsional stiffness modifier. As such, it is recommended to use nonlinear layered shells for modelling monolithic RC two-way slabs. Regarding the mesh size, it is recommended to use a square mesh size with a side length of $L/10$ – $L/20$ for this type of slab, with L representing the centreline-to-centreline distance of adjacent columns supporting a bay.
- The dynamic amplification factor (DAF) obtained from the pseudo-static approach (energy-conservation principle) shows a different trend than that is assumed in current codes. The difference comes from the fact that the codes assume an elastic-perfectly-plastic (EPP) model, whereas the actual response (as considered in the pseudo-static approach) accounts for the increase of resistance from catenary mechanisms. Such discrepancies can lead to unconservative (lower) DAF values for the codes. Such discrepancies have also been studied by other researchers (e.g. [56,58]), indicating that guidelines and standards can underestimate DAF values, leading to unconservative predictions.
- Comparing six different locations of removed columns in the three investigated building samples, the indexes consistently agreed that the removal of a specific penultimate–internal column (Internal-1) is the most critical one. This is mainly because the corresponding column has a high level of gravity loading (large tributary area) while having relatively weak lateral restraints due to being located relatively close to the free edges of the building. Consequently, the development of the catenary and tensile membrane actions during large deformation stages was rather limited.
- Comparing the three building designs, Indexes 1-3 consistently valued Building B with a longer span length as having the lowest residual capacity after initial column failure. As the span becomes longer, the tributary area for each column becomes proportionally larger, and hence, more loads must be redistributed from the failed column to its surroundings to achieve a new equilibrium state.
- Contrarily to the other indexes evaluated, Index 4 suggests that Building C is least robust. This index provides useful information on the critical failure path (sequence of column losses) that can trigger collapse. In this study, all three buildings can withstand two-column losses without collapsing, but the critical path of each building is unique. The critical path for Building B, with a longer span, mainly crosses the inner part of the buildings where the tributary area is the largest, whereas, for Buildings A and C, the critical path mainly crosses the perimeter and corner parts of the building. The critical path of Building C leads to collapse before that of Buildings A and B, explaining why it is deemed as the least robust according to this index.
- Considering the time and effort required to perform the analysis and the versatility of the index, it can be concluded that Index 2 is the most practical to use for most applications. It requires only a nonlinear static pushdown that is less time-consuming than the dynamic analysis, yet it indirectly accounts for the dynamic effect through the energy-based principle. However, evaluating a system through the lens of multiple robustness indexes proved to provide a more complete picture of system performance compared to relying solely on a single index and, therefore, suggested.
- Two potential applications of the robustness index (Index 2) have been presented: 1) relating the global (system) robustness index to the local damage state of individual structural components; 2) comparing and evaluating different retrofitting solutions. These two demonstrations suggest that combining efficient modelling strategy and suitable robustness indexes can be a very useful and versatile decision-making tool for practising engineers.

CRediT authorship contribution statement

Andri Setiawan: Writing – review & editing, Writing – original draft, Visualization, Validation, Methodology, Investigation, Formal analysis, Data curation, Conceptualization. **Diego Cetina:** Software, Investigation, Formal analysis, Data curation. **Nirvan Makoond:** Writing – review & editing, Writing – original draft, Formal analysis, Data curation. **Manuel Buitrago:** Writing – review & editing, Supervision, Methodology, Investigation, Conceptualization. **Jose Miguel Adam:** Writing – review & editing, Supervision, Resources, Funding acquisition.

Declaration of Competing Interest

The authors declare that they have no known competing financial interests or personal relationships that could have appeared to influence the work reported in this paper.

Acknowledgements

This article is part of a project (*Endure*) that has received funding from the European Research Council (ERC) under the European Union's Horizon 2020 research and innovation programme (Grant agreement No. 101000396). The authors would also like to express their gratitude for funding received under the postdoctoral programs of the Generalitat Valenciana/Fons Social Europeu [CIAPOS/2023/216] and for the *Evolve* project (ref. CIGE/2023/199).

Appendix A. Supporting information

Supplementary data associated with this article can be found in the online version at doi:10.1016/j.istruc.2024.107898.

References

[1] United Nations Office for Disaster Risk Reduction (UNDRR). Principles for resilient infrastructure; 2022.
[2] Arup, Review of International Research on Structural Robustness and Disproportionate Collapse. UK Government: Department for Communities and Local Government; 2011.
[3] Adam JM, Parisi F, Sagaseta J, Lu X. Research and practice on progressive collapse and robustness of building structures in the 21st century. Eng Struct 2018;173: 122–49. https://doi.org/10.1016/j.engstruct.2018.06.082.
[4] Russell JM, Sagaseta J, Cormie D, Jones AEK. Historical review of prescriptive design rules for robustness after the collapse of Ronan Point. Structures 2019;20: 365–73. https://doi.org/10.1016/j.istruc.2019.04.011.
[5] European Committee for Standardization (CEN). EN 1991–1-7:2006: Eurocode 1 - Actions on structures - Part 1–7: General actions - accidental actions; 2006.
[6] Department of Defense (DoD). UFC 4–023-03: Design of Buildings To Resist Progressive Collapse; 2016.
[7] American Society of Civil Engineers (ASCE). ASCE/SEI 76–23: Standard for Mitigation of Disproportionate Collapse Potential in Buildings and Other Structures. Reston, VA: American Society of Civil Engineers; 2023. ⟨https://doi.org/10.1061/9780784415931⟩.
[8] National Institute of Standards and Technology (NIST). NISTIR 7396: Best practices for reducing the potential for progressive collapse in buildings 2007:216.
[9] Starossek U. Measures of robustness and collapse resistance. Progressive Collapse of Structures. ICE Publishing,; 2017. p. 129–40. https://doi.org/10.1680/pcos.61682.129.
[10] Jiang J, Zhang Q, Li L, Chen W, Ye J, Li GQ. Review on quantitative measures of robustness for building structures against disproportionate collapse. Int J High-Rise Build 2020;9:127–54. https://doi.org/10.21022/IJHRB.2020.9.2.127.
[11] Kunnath SK, Bao Y, El-Tawil S. Advances in computational simulation of gravity-induced disproportionate collapse of RC frame buildings. J Struct Eng 2018;144: 03117003. https://doi.org/10.1061/(ASCE)ST.1943-541X.0001938.
[12] Bao Y, Kunnath SK, El-Tawil S, Lew HS. Macromodel-based simulation of progressive collapse: RC frame structures. J Struct Eng 2008;134:1079–91. https://doi.org/10.1061/(ASCE)0733-9445(2008)134:7(1079).
[13] Menchel K, Massart TJ, Rammer Y, Bouillard P. Comparison and study of different progressive collapse simulation techniques for RC structures. J Struct Eng 2009; 135:685–97. https://doi.org/10.1061/(ASCE)0733-9445(2009)135:6(685).
[14] Sasani M, Kazemi A, Sagiroglu S, Forest S. Progressive collapse resistance of an Actual 11-story structure subjected to severe initial damage. J Struct Eng 2011; 137:893–902. https://doi.org/10.1061/(ASCE)ST.1943-541X.0000418.
[15] Brunesi E, Nascimbene R. Extreme response of reinforced concrete buildings through fiber force-based finite element analysis. Eng Struct 2014;69:206–15. https://doi.org/10.1016/j.engstruct.2014.03.020.
[16] Parisi F, Scalvenzi M. Progressive collapse assessment of gravity-load designed European RC buildings under multi-column loss scenarios. Eng Struct 2020;209: 110001. https://doi.org/10.1016/j.engstruct.2019.110001.
[17] Bao Y, Main JA, Noh S-Y. Evaluation of structural robustness against column loss: methodology and application to RC frame buildings. J Struct Eng 2017;143. https://doi.org/10.1061/(ASCE)ST.1943-541X.0001795.
[18] Alashker Y, Li H, El-Tawil S. Approximations in progressive collapse modeling. J Struct Eng 2011;137:914–24. https://doi.org/10.1061/(ASCE)ST.1943-541X.0000452.
[19] Sasani M, Werner A, Kazemi A. Bar fracture modeling in progressive collapse analysis of reinforced concrete structures. Eng Struct 2011;33:401–9. https://doi.org/10.1016/j.engstruct.2010.10.023.
[20] Pekau OA, Cui Y. Progressive collapse simulation of precast panel shear walls during earthquakes. Comput Struct 2006;84:400–12. https://doi.org/10.1016/j.compstruc.2005.09.027.
[21] Živaljić N, Nikolić Ž, Smoljanović H. Computational aspects of the combined finite–discrete element method in modelling of plane reinforced concrete structures. Eng Fract Mech 2014;131:669–86. https://doi.org/10.1016/j.engfracmech.2014.10.017.
[22] Lu Z, He X, Zhou Y. Discrete element method-based collapse simulation, validation and application to frame structures. Struct Infrastruct Eng 2018;14:538–49. https://doi.org/10.1080/15732479.2017.1373133.
[23] Buitrago M, Setiawan A, Makoond N, Gerbaudo ML, Marin L, Cetina D, et al. Failure analysis after the progressive collapse of a precast building. Eng Struct 2024;321:118893. https://doi.org/10.1016/j.engstruct.2024.118893.
[24] Makoond N, Setiawan A, Orton SL, Adam JM. The effect of continuity reinforcement on the progression of collapse in reinforced concrete buildings. Structures 2024;61:105981. https://doi.org/10.1016/j.istruc.2024.105981.
[25] Makoond N, Setiawan A, Buitrago M, Adam JM. Arresting failure propagation in buildings through collapse isolation. Nature 2024;629:592–6. https://doi.org/10.1038/s41586-024-07268-5.
[26] TAGEL-DIN H, MEGURO K. Nonlinear simulation of RC structures using applied element method. Doboku Gakkai Ronbunshu 2000;2000:13–24. https://doi.org/10.2208/jscej.2000.654_13.
[27] Grunwald C, Khalil AA, Schaufelberger B, Ricciardi EM, Pellecchia C, De Iuliis E, et al. Reliability of collapse simulation – comparing finite and applied element method at different levels. Eng Struct 2018;176:265–78. https://doi.org/10.1016/j.engstruct.2018.08.068.
[28] Starossek U, Haberland M. Measures of structural robustness — requirements and applications. Structures Congress 2008. Reston, VA: American Society of Civil Engineers,; 2008. p. 1–10. https://doi.org/10.1061/41016(314)235.
[29] Stochino F, Bedon C, Sagaseta J, Honfi D. Robustness and resilience of structures under extreme loads. Adv Civ Eng 2019;2019:1–14. https://doi.org/10.1155/2019/4291703.
[30] Makoond N, Setiawan A, Buitrago M, Adam JM. Arresting failure propagation in buildings through collapse isolation. Nature 2024;629:592–6. https://doi.org/10.1038/s41586-024-07268-5.
[31] Mucedero G, Brunesi E, Parisi F. Nonlinear material modelling for fibre-based progressive collapse analysis of RC framed buildings. Eng Fail Anal 2020;118. https://doi.org/10.1016/j.engfailanal.2020.104901.
[32] American Society of Civil Engineers (ASCE). .. ASCE/SEI 41-23: Seismic Evaluation and Retrofit of Existing Buildings. American Society of Civil Engineers,; 2023. https://doi.org/10.1061/9780784416112.
[33] Federal Emergency Management Agency (FEMA). FEMA 356: Prestandard and Commentary for the Seismic Rehabilitation of Buildings; 2000.
[34] Cetina D, Setiawan A, Makoond N, Buitrago M, Adam JM. Simplified modelling strategy for evaluating failure propagation in reinforced concrete structures. Construction Pathology, 2024. REHABEND: Rehabilitation Technology and Heritage Management,; 2024.
[35] Elghazouli A.Y., Izzuddin B.A., Richardson A.J. Numerical Modelling of the Structural "Re Behaviour of Composite Buildings. vol. 35; 2000.
[36] Setiawan A, Vollum RL, Macorini L, Izzuddin BA. Punching shear design of RC flat slabs supported on wall corners. Struct Concr 2020;21:859–74. https://doi.org/10.1002/suco.201900514.
[37] Setiawan A, Vollum RL, Macorini L, Izzuddin BA. Punching of RC slabs without transverse reinforcement supported on elongated columns. Structures 2020;27: 2048–68. https://doi.org/10.1016/j.istruc.2020.08.017.
[38] Setiawan A, Vollum RL, Macorini L, Izzuddin B. Efficient 3-D modelling of punching shear failure at slab-column connections by means of nonlinear joint elements. Eng Struct 2019;197. https://doi.org/10.1016/j.engstruct.2019.109372.
[39] Liel AB, Asce M, Haselton CB, Deierlein GG, Asce F. Seism Collapse Saf Reinf Concr Build Ii: Comp Assess Nonductile Ductile Moment Fram 2011. https://doi.org/10.1061/(ASCE)ST.1943-541X.
[40] European Committee for Standardization (CEN). EN 1992–1-1: Eurocode 2: Design of concrete structures - Part 1–1: General rules and rules for buildings. 2004.
[41] European Committee for Standardization (CEN). Eurocode 8: Design Provisions for Earthquake Resistance of Structures: part. 1-3: General Rules, Specific Rules for Various Materials and Element.. London: BSI,; 1996.
[42] CSI. SAP2000 Integrated Software for Structural Analysis and Design 2024.
[43] Deng X-F, Liang, Shi-Lin FuF, Asce F, Qian K, Asce M. Effects of High-Strength Concrete on Progressive Collapse Resistance of Reinforced Concrete Frame 2020. J Struct Eng 2020. https://doi.org/10.1061/(ASCE)ST.1943.
[44] Zhou Y, Hu X, Pei Y, Hwang HJ, Chen T, Yi W, et al. Dynamic load test on progressive collapse resistance of fully assembled precast concrete frame structures. Eng Struct 2020;214. https://doi.org/10.1016/j.engstruct.2020.110675.
[45] Qian K, Li B. Dynamic and residual behavior of reinforced concrete floors following instantaneous removal of a column. Eng Struct 2017;148:175–84. https://doi.org/10.1016/j.engstruct.2017.06.059.

[46] Makoond N, Setiawan A, Orton SL, Adam JM. The effect of continuity reinforcement on the progression of collapse in reinforced concrete buildings. Structures 2024;61. https://doi.org/10.1016/j.istruc.2024.105981.

[47] Buitrago M, Bertolesi E, Sagaseta J, Calderón PA, Adam JM. Robustness of RC building structures with infill masonry walls: tests on a purpose-built structure. Eng Struct 2021;226. https://doi.org/10.1016/j.engstruct.2020.111384.

[48] Darwin D, Pecknold DAW. Inelast Model Cycl Biaxial Load Reinf Concr 1974.

[49] The modified compression-field theory for reinforced concrete elements subjected to shear. ACI J Proc 1986;83. https://doi.org/10.14359/10416.

[50] MPA - The Concrete Centre. How to design reinforced concrete flat slabs using Finite Element Analysis. 2006.

[51] Khandelwal K, El-Tawil S. Pushdown resistance as a measure of robustness in progressive collapse analysis. Eng Struct 2011;33:2653–61. https://doi.org/10.1016/j.engstruct.2011.05.013.

[52] Bao Y, Asce AM, Main JA, Asce M, Noh S-Y. Evaluation of structural robustness against column loss: methodology and application to rc frame buildings. J Struct Eng 2017. https://doi.org/10.1061/(ASCE).

[53] Fallon CT, Quiel SE, Naito CJ. Uniform pushdown approach for quantifying building-frame robustness and the consequence of disproportionate collapse. J Perform Constr Facil 2016;30. https://doi.org/10.1061/(asce)cf.1943-5509.0000912.

[54] Fascetti A, Kunnath SK, Nisticò N. Robustness evaluation of RC frame buildings to progressive collapse. Eng Struct 2015;86:242–9. https://doi.org/10.1016/j.engstruct.2015.01.008.

[55] European Committee for Standardization (CEN). EN 1991–1-1: Eurocode 1: Actions on structures - Part 1–1: General actions - Densities, self-weight, imposed loads for buildings. 1991.

[56] Izzuddin BA, Vlassis AG, Elghazouli AY, Nethercot DA. Progressive collapse of multi-storey buildings due to sudden column loss - part I: simplified assessment framework. Eng Struct 2008;30:1308–18. https://doi.org/10.1016/j.engstruct.2007.07.011.

[57] McKay A, Marchand K, Williamson E, Crowder B, Stevens D. Dynamic and nonlinear load increase factors for collapse design and analysis. Proc Int Symp Interact Eff Munitions Struct (ISIEMS) 2007;12.

[58] Izzuddin BA. Rational robustness design of multistory building structures. J Struct Eng 2022;148. https://doi.org/10.1061/(asce)st.1943-541x.0003254.

[59] Sio J, Izzuddin BA. Enhanced rational horizontal tying force method for practical robustness design of building structures. Eng Struct 2024;301. https://doi.org/10.1016/j.engstruct.2023.117268.

[60] Izzuddin BA, Sio J. Rational horizontal tying force method for practical robustness design of building structures. Eng Struct 2022;252. https://doi.org/10.1016/j.engstruct.2021.113676.

[61] Parisi F, Scalvenzi M, Brunesi E. Performance limit states for progressive collapse analysis of reinforced concrete framed buildings. Struct Concr 2019;20:68–84. https://doi.org/10.1002/suco.201800039.

[62] M. Mahoney R.D. Hanson FEMA P-58-1: Seism Perform Assess Build Vol 1-Methodol Second Ed; 2018.